Supplementary Material

Cyanine–cyanine hybrid structure as a stabilized polyelectrochromic system: synthesis, stabilities, and redox behavior of di(1-azulenyl)methylium units connected with electron-accepting π-electron systems

Shunji Ito,[*,†] Ryuta Sekiguchi,[‡] Akira Mizushima,[†] Kohei Kudo,[†] Jun Kawakami,[†] and Taku Shoji[‡]

[†] *Graduate School of Science and Technology, Hirosaki University, Hirosaki 036-8561, Aomori, Japan*

[‡] *Department of Chemistry, Faculty School of Science, Shinshu University, Matsumoto 390-8621, Nagano, Japan*

Email: itsnj@hirosaki-u.ac.jp

Table of Contents

1. Experimental details for physical measurements

pK_R^+ Value Measurements: Sample solutions of the hexafluorophosphates **5a**$^+PF_6^-$, **8a**$^+PF_6^-$, **11a**–**d**$^+PF_6^-$, and **14**$^+PF_6^-$ were prepared by dissolving 1–2 mg of the hexafluorophosphates in MeCN and a glycine (0.1 M) solution (50 mL) and made up to 100 mL by further adding MeCN; the sample solution with lower acidity was made by further alkalification with 20% aqueous NaOH. For the preparation of a sample solution of the hexafluorophosphates **5b**$^+PF_6^-$ and **8b**$^+PF_6^-$, buffer solutions of slightly different acidities were prepared by mixing CH_3COONa (1 M) and HCl (1 M) for pH 1.0–3.0, CH_3COONa (0.1 M) and CH_3COOH (0.1 M) for pH 3.2–5.0, KH_2PO_4 (0.1 M) and $Na_2B_4O_7$ (0.05 M) for pH 6.0–9.0, $Na_2B_4O_7$ (0.05 M) and Na_2CO_3 (0.05 M) for pH 10.0, and $Na_2B_4O_7$ (0.05 M) and NaOH (0.1 M) for pH 11.0–11.4, in various portions. Each 1 mL portion of the stock solution, prepared by dissolving 2–3 mg of the hexafluorophosphates **5b**$^+PF_6^-$ and **8b**$^+PF_6^-$ in MeCN (20 mL), was pipetted out and made up to 10 mL by adding an appropriate buffer solution (5 mL) and MeCN. The pH of each sample was made on a Horiba pH meter F-13 calibrated with standard buffers before use. The observed absorbance at the specific absorption maxima in visible region of the cations **5a**$^+$, **5b**$^+$, **8a**$^+$, **8b**$^+$, **11a**–**d**$^+$, and **14**$^+$ were plotted against the pH, giving classical titration curves whose midpoints were taken as the pK_R^+ values.

Voltammetry Measurements: The voltammetry measurements were carried out on a ALS 610B electrochemical analyzer in benzonitrile containing Et_4NClO_4 (0.1 M) as a supporting electrolyte utilizing Pt working and auxiliary electrodes, and a reference electrode formed from $Ag/AgNO_3$ (0.01 M) in acetonitrile containing *n*-Bu_4NClO_4 (0.1 M) at the scan rate of 100 mV s^{-1}. The internal reference Fc/Fc^+ discharges at +0.15 V under these conditions.

Spectroelectrogram Measurements: Sample solutions were prepared by dissolving **5a**$^+PF_6^-$, **5b**$^+PF_6^-$, **8a**$^+PF_6^-$, **8b**$^+PF_6^-$, **11a**–**d**$^+PF_6^-$, and **14**$^+PF_6^-$ in benzonitrile containing Et_4NClO_4 (0.1 M) and were degassed through an Ar stream. Spectroelectrogram measurements were carried out using a quarts cell (1 × 10 × 35 mm) equipped with a Pt mesh and a wire as the working and counter electrodes, respectively, which were separated by a glass filter. A constant-current reduction and oxidation were applied to the sample solution. The electrical current was monitored by a microampere meter. The potential values are automatically increased by the resistance of the sample solution from 0 V up to ±12 V by our constant current apparatus. Spectroelectrograms were measured on an Ocean Optics USB2000 spectrophotometer.

2. pK_a^+ data of 5a⁺, 5b⁺, 8a⁺, 8b⁺, 11a–d⁺, and 14⁺

Table S1. pK_R^+ Values [a] of **5a**$^+$, **5b**$^+$, **8a**$^+$, **8b**$^+$, **11a–d**$^+$, and **14**$^+$

Sample	pK_R^{+} [b]	Sample	pK_R^{+} [b]
5a$^+$	9.5 ± 0.1 (1%)	**11a**$^+$	12.1 ± 0.1 (5%)
5b$^+$	1.4 ± 0.1 (89%)	**11b**$^+$	5.3 ± 0.1 (60%)
8a$^+$	10.9 ± 0.1 (3%)	**11c**$^+$	11.7 ± 0.1 (5%)
8b$^+$	2.9 ± 0.1 (83%)	**11d**$^+$	8.7 ± 0.1 (1%)
		14$^+$	9.3 ± 0.1 (10%)

[a] The pK_R^+ values were determined spectrophotomerically in a buffered solution prepared in 50% aqueous acetonitrile. [b] Regenerated absorption maxima (%) of the cations in visible region by acidification of the alkaline solution with HCl are shown in parentheses.

(a)

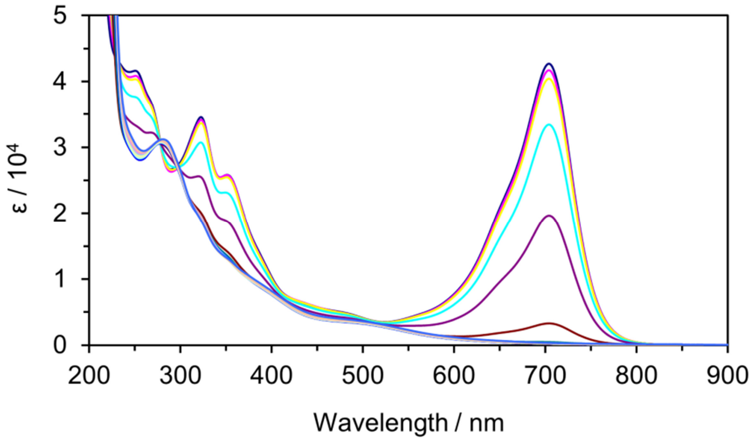

(b)

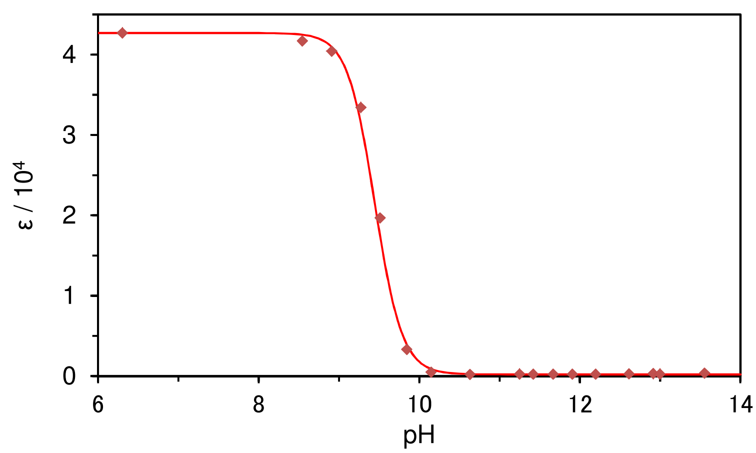

Figure S1. Continuous change in UV/Vis spectra of **5a**$^{+}$: (a) change in UV/Vis spectra and (b) a plot of pH vs. absorbance at the longest wavelength absorption maximum in base titration in 50% water/acetonitrile solution.

(a)

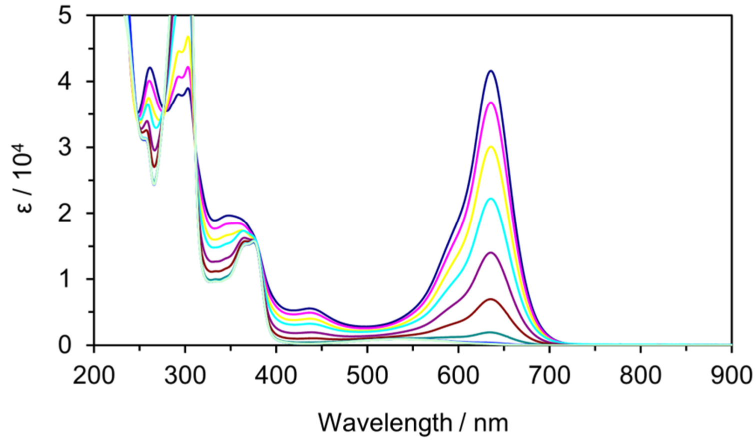

(b)

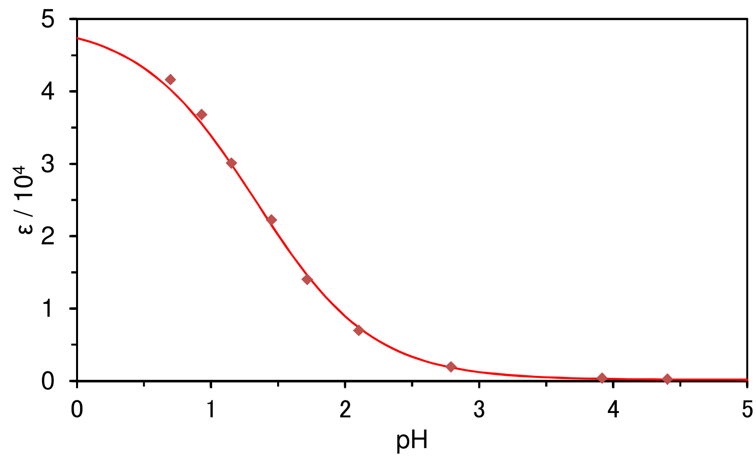

Figure S2. Continuous change in UV/Vis spectra of **5b**$^{+}$: (a) change in UV/Vis spectra and (b) a plot of pH vs. absorbance at the longest wavelength absorption maximum in base titration in 50% water/acetonitrile solution.

(a)

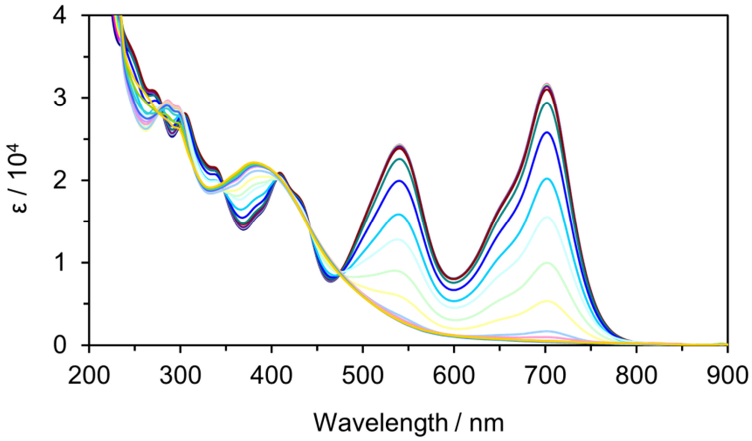

(b)

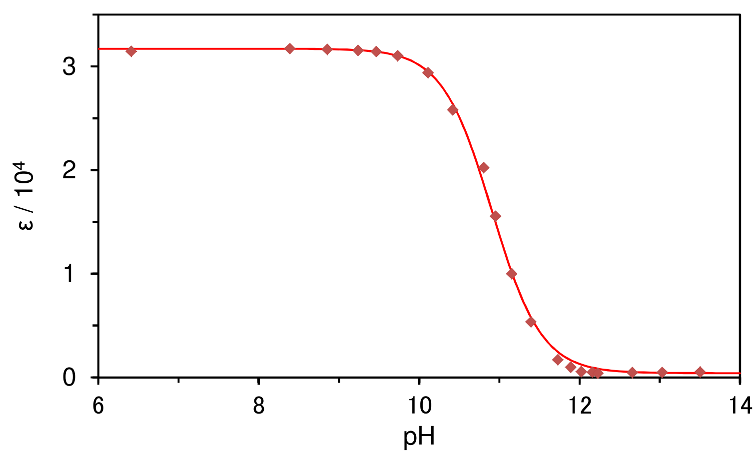

Figure S3. Continuous change in UV/Vis spectra of **8a**$^{+}$: (a) change in UV/Vis spectra and (b) a plot of pH vs. absorbance at the longest wavelength absorption maximum in base titration in 50% water/acetonitrile solution.

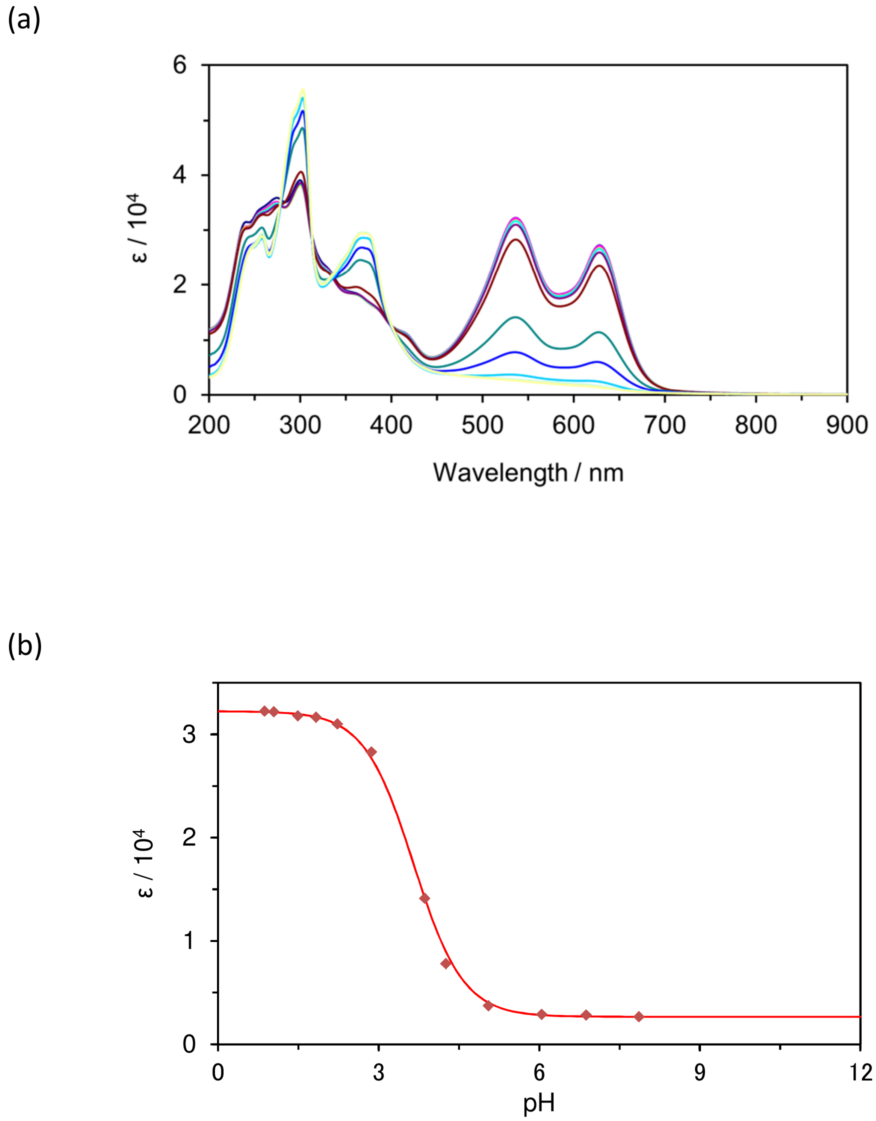

Figure S4. Continuous change in UV/Vis spectra of **8b**$^+$: (a) change in UV/Vis spectra and (b) a plot of pH vs. absorbance at the longest wavelength absorption maximum in base titration in 50% water/acetonitrile solution.

(a)

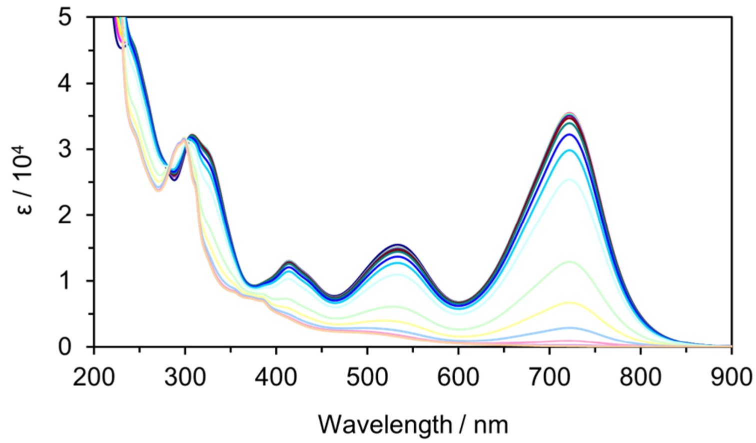

(b)

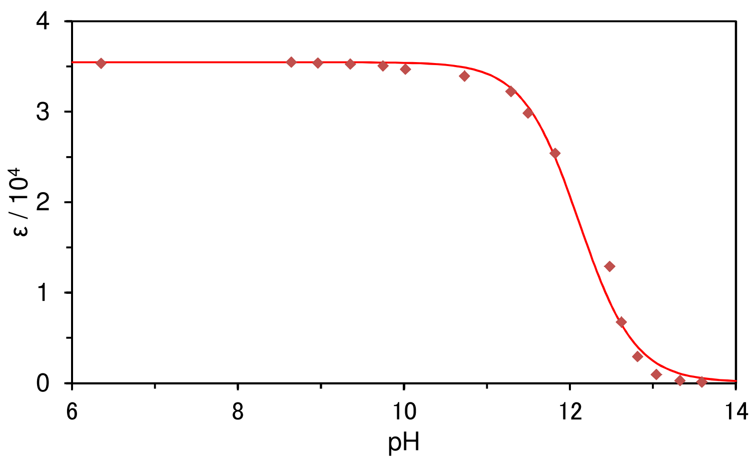

Figure S5. Continuous change in UV/Vis spectra of **11a**$^{+}$: (a) change in UV/Vis spectra and (b) a plot of pH vs. absorbance at the longest wavelength absorption maximum in base titration in 50% water/acetonitrile solution.

(a)

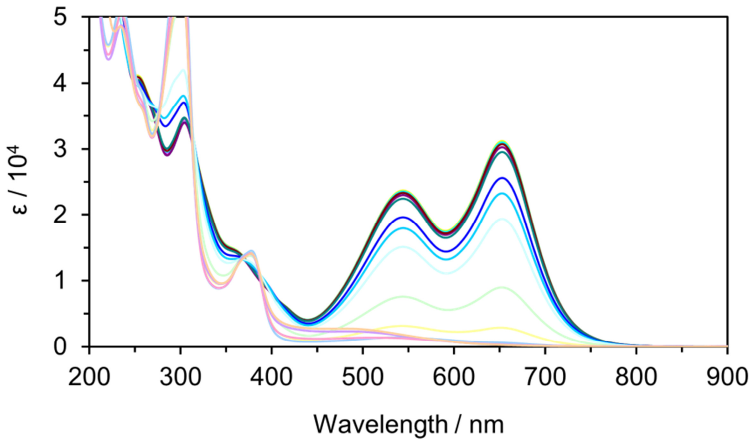

(b)

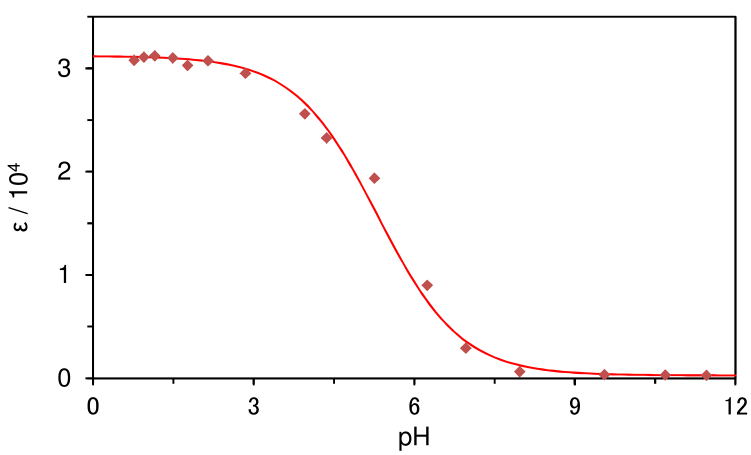

Figure S6. Continuous change in UV/Vis spectra of **11b**$^{+}$: (a) change in UV/Vis spectra and (b) a plot of pH vs. absorbance at the longest wavelength absorption maximum in base titration in 50% water/acetonitrile solution.

(a)

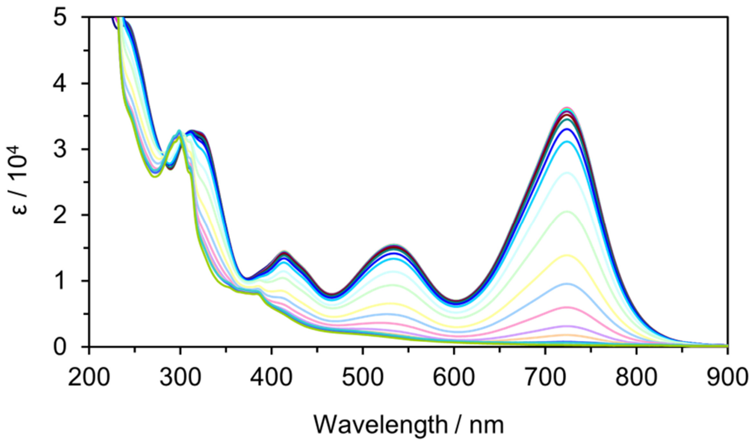

(b)

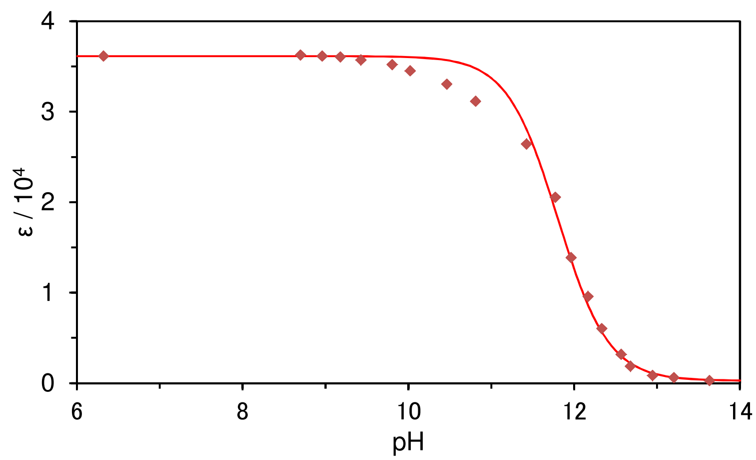

Figure S7. Continuous change in UV/Vis spectra of **11c**$^{+}$: (a) change in UV/Vis spectra and (b) a plot of pH vs. absorbance at the longest wavelength absorption maximum in base titration in 50% water/acetonitrile solution.

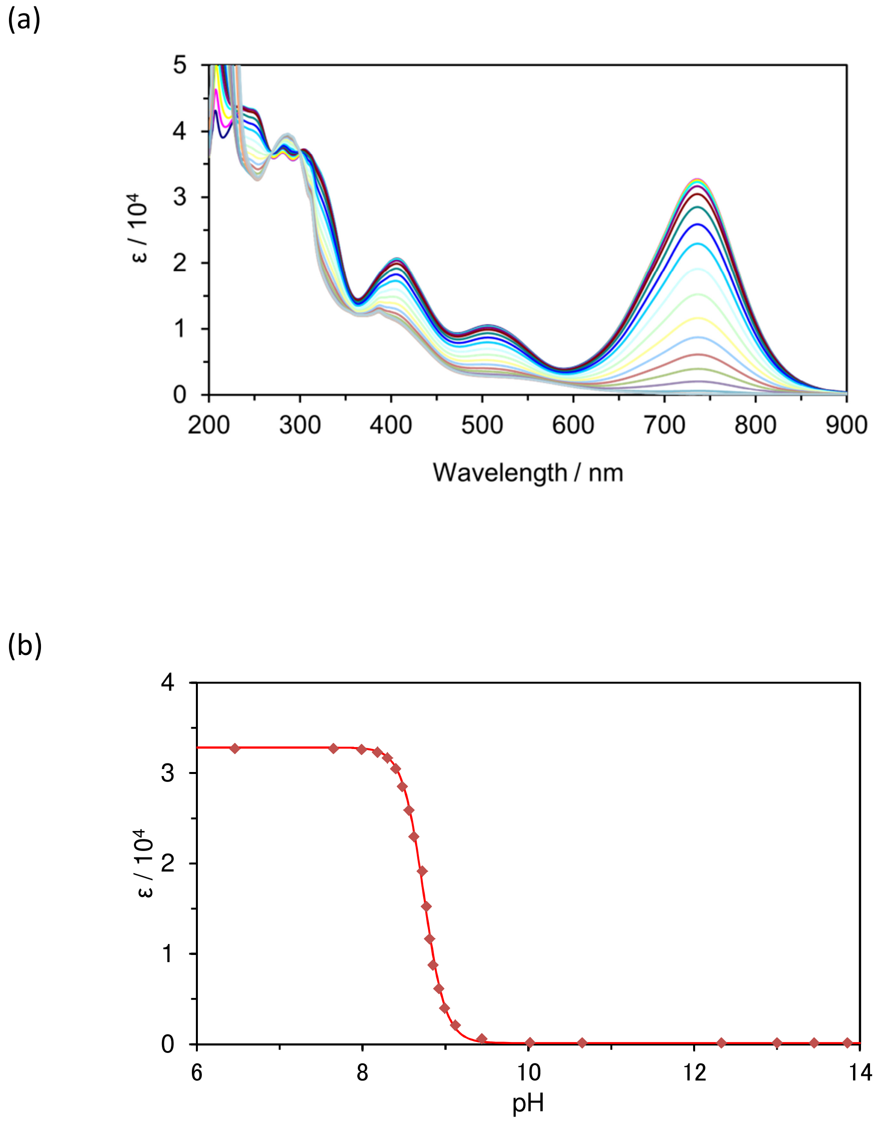

Figure S8. Continuous change in UV/Vis spectra of **11d**$^+$: (a) change in UV/Vis spectra and (b) a plot of pH vs. absorbance at the longest wavelength absorption maximum in base titration in 50% water/acetonitrile solution.

(a)

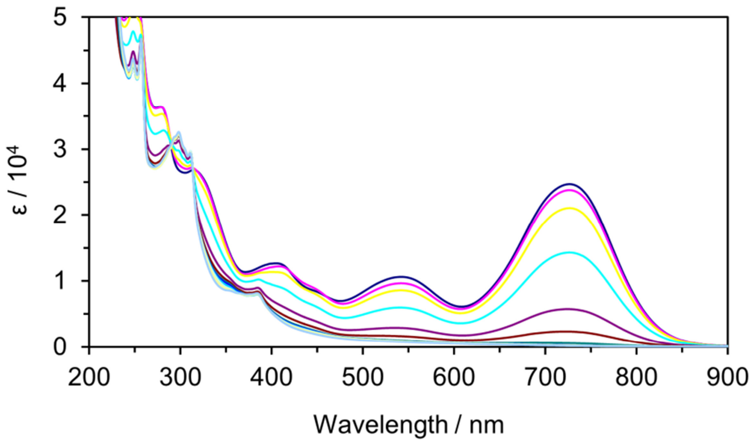

(b)

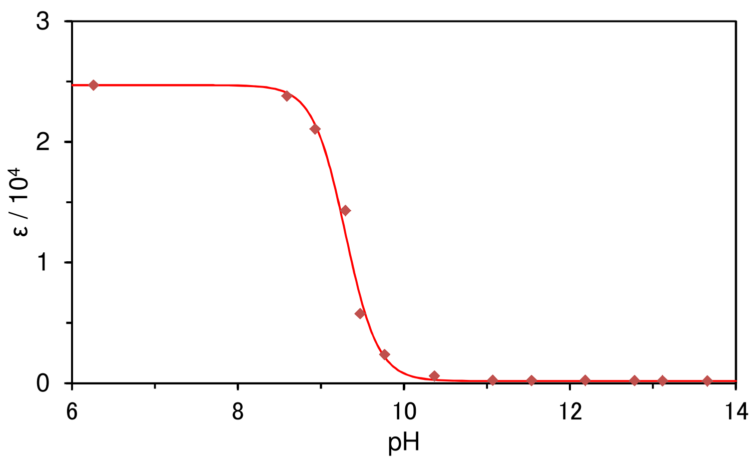

Figure S9. Continuous change in UV/Vis spectra of **14**$^+$: (a) change in UV/Vis spectra and (b) a plot of pH vs. absorbance at the longest wavelength absorption maximum in base titration in 50% water/acetonitrile solution.

3. CV and DPV waves of 5a$^+$, 5b$^+$, 8a$^+$, 8b$^+$, 11a–d$^+$, and 14$^+$

Table S2. Reduction potentials [a] of **5a**$^+$, **5b**$^+$, **8a**$^+$, **8b**$^+$, **11a–d**$^+$, and **14**$^+$

Sample	E_1^{red}	E_2^{red}	E_3^{red}	E_4^{red}	E_5^{red}	E_6^{red}
5a$^+$	−0.59	−0.94	(−2.14)			
	(−0.55)	(−0.92)	(−2.09)			
5b$^+$	−0.31	−0.79	(−1.47)	(−1.74)	(−1.77)	
	(−0.28)	(−0.76)	(−1.44)	(−1.68)	(−1.76)	
8a$^+$	−0.63	−1.08	(−1.97)	(−2.08)		
	(−0.61)	(−1.06)	(−1.94)	(−2.03)	(−2.16)	
8b$^+$	−0.36	−0.99	(−1.42)	(−1.67)	(−1.76)	
	(−0.34)	(−0.96)	(−1.38)	(−1.63)	(−1.74)	(−2.02)
11a$^+$	−0.67	(−1.48)				
	(−0.64)	(−1.45)	(−2.03)	(−2.16)		
11b$^+$	−0.37	(−1.19)	(−1.54)	(−1.64)	(−1.77)	
	(−0.34)	(−1.15)	(−1.51)	(−1.60)	(−1.74)	
11c$^+$	−0.65	(−1.54)				
	(−0.62)	(−1.42)	(−1.87)	(−2.02)	(−2.16)	
11d$^+$	−0.50	−0.86	(−1.57)	(−1.87)		
	(−0.48)	(−0.84)	(−1.54)	(−1.84)	(−2.04)	(−2.15)
14$^+$	−0.49	(−1.12)				
	(−0.47)	(−1.08)	(−1.92)	(−2.00)	(−2.11)	(−2.22)

[a] Redox potentials were measured by CV and DPV [V vs. Ag/$AgNO_3$, 1 mM in benzonitrile containing Et_4NClO_4 (0.1 M), Pt electrode (ID: 1.6 mm), scan rate 100 mV s^{-1}, and Fc/Fc^+ = +0.15 V]. The peak potentials measured by DPV are shown in the second line with parentheses.

Table S3. Oxidation potentials[a] of **5a**$^+$, **5b**$^+$, **8a**$^+$, **8b**$^+$, **11a–d**$^+$, and **14**$^+$

Sample	E_1^{ox}	E_2^{ox}	E_3^{ox}	E_4^{ox}
5a$^+$	+0.94	(+1.44)		
	(+0.92)	(+1.41)		
5b$^+$	(+1.38)			
	(+1.35)			
8a$^+$	+0.95	(+1.33)	(+1.54)	(+1.71)
	(+0.93)	(+1.29)	(+1.48)	(+1.64)
8b$^+$	(+1.43)	(+1.76)		
	(+1.36)	(+1.68)		
11a$^+$	+0.84	(+1.40)		
	(+0.82)	(+1.30)		
11b$^+$	(+1.27)	(+1.62)		
	(+1.24)	(+1.59)	(+1.77)	
11c$^+$	+0.85			
	(+0.82)	(+1.41)	(+1.50)	
11d$^+$	+0.88			
	(+0.86)	(+1.38)	(+1.64)	
14$^+$	+0.93	(+1.48)		
	(+0.90)	(+1.41)		

[a] Redox potentials were measured by CV and DPV [V vs. Ag/$AgNO_3$, 1 mM in benzonitrile containing Et_4NClO_4 (0.1 M), Pt electrode (ID: 1.6 mm), scan rate 100 mV s^{-1}, and Fc/Fc^+ = +0.15 V]. The peak potentials measured by DPV are shown in the second line with parentheses.

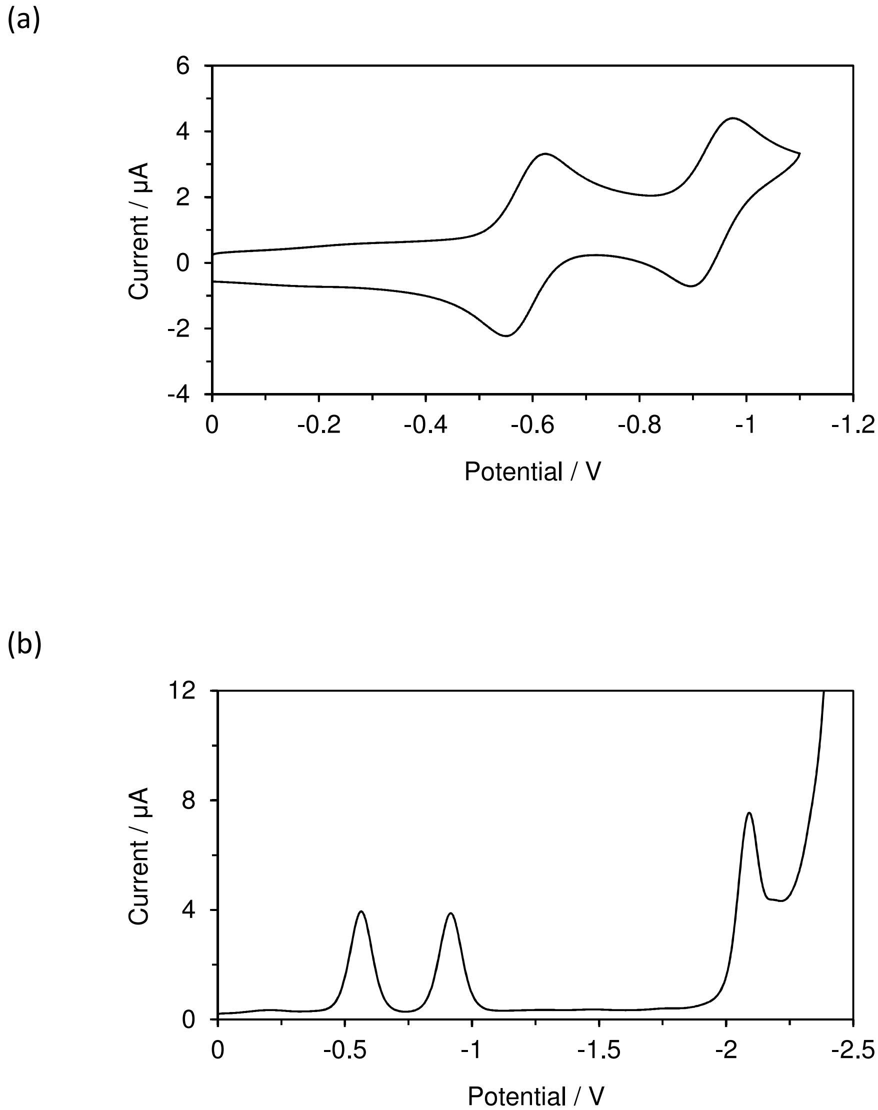

Figure S10. Voltammograms of **5a**$^{+}$: (a) reduction wave on CV and (b) reduction wave of on DPV in benzonitrile (1 mM) containing Et_4NClO_4 (0.1 M) as a supporting electrolyte; scan rate, 100 mV s^{-1}.

(a)

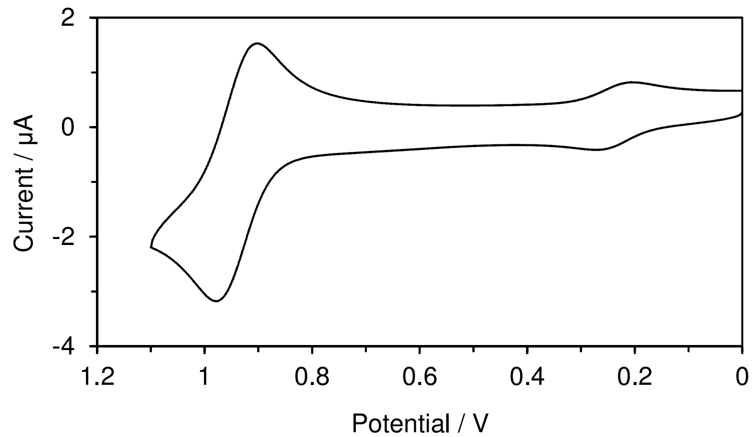

(b)

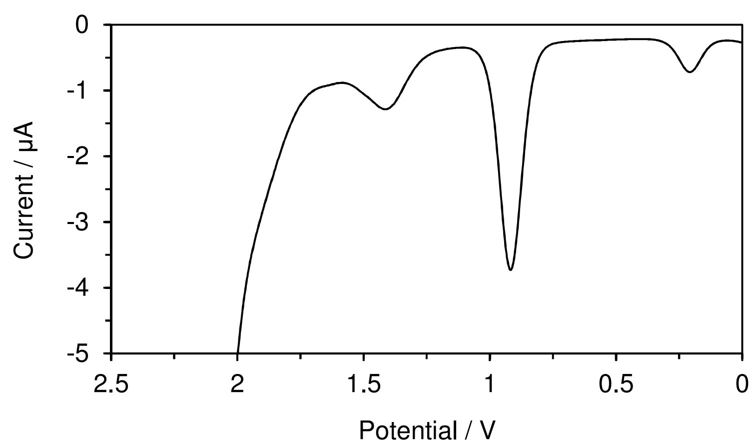

Figure S11. Voltammograms of **5a**$^{+}$: (a) oxidation wave on CV and (b) oxidation wave on DPV in benzonitrile (1 mM) containing Et_4NClO_4 (0.1 M) as a supporting electrolyte; scan rate, 100 mV s^{-1}.

(a)

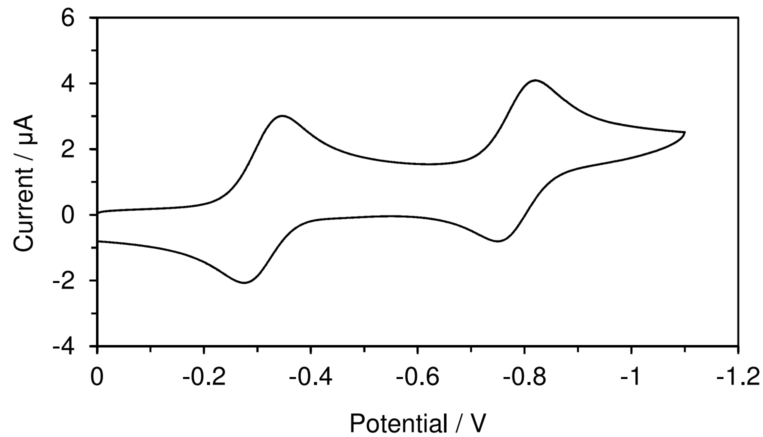

(b)

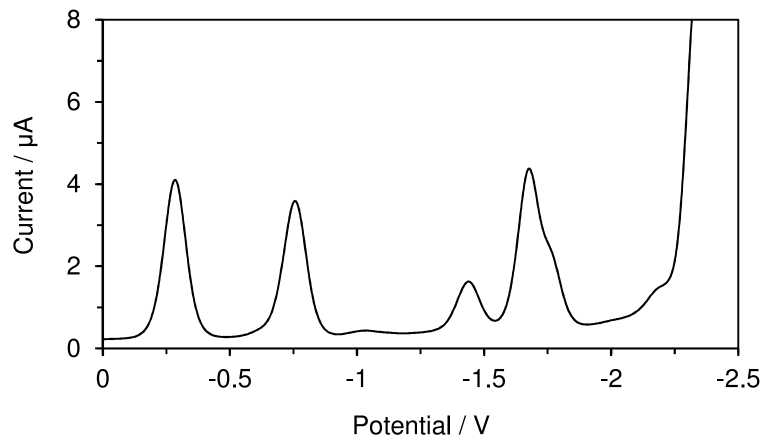

Figure S12. Voltammograms of **5b**$^{+}$: (a) reduction wave on CV and (b) reduction wave on DPV in benzonitrile (1 mM) containing Et_4NClO_4 (0.1 M) as a supporting electrolyte; scan rate, 100 mV s^{-1}.

(a)

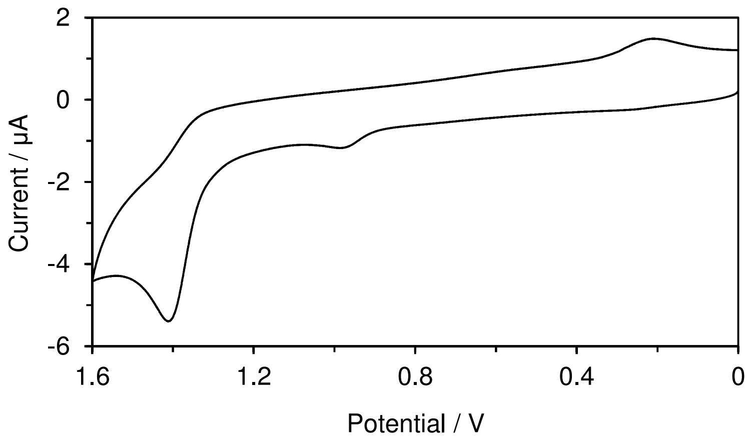

(b)

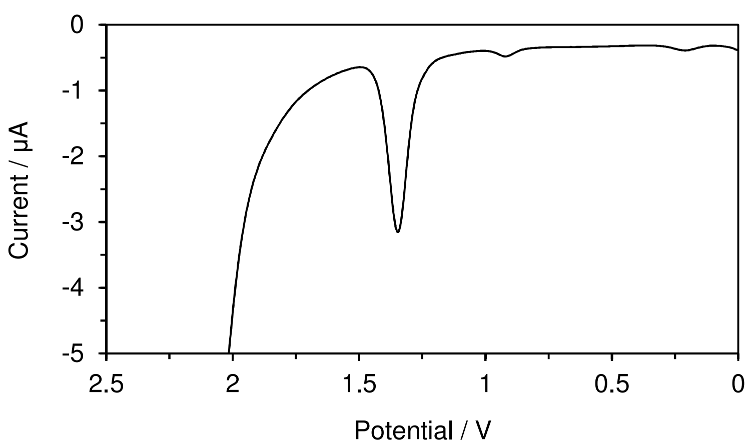

Figure S13. Voltammograms of **5b**$^+$: (a) reduction wave on CV and (b) oxidation wave on DPV in benzonitrile (1 mM) containing Et_4NClO_4 (0.1 M) as a supporting electrolyte; scan rate, 100 mV s^{-1}.

(a)

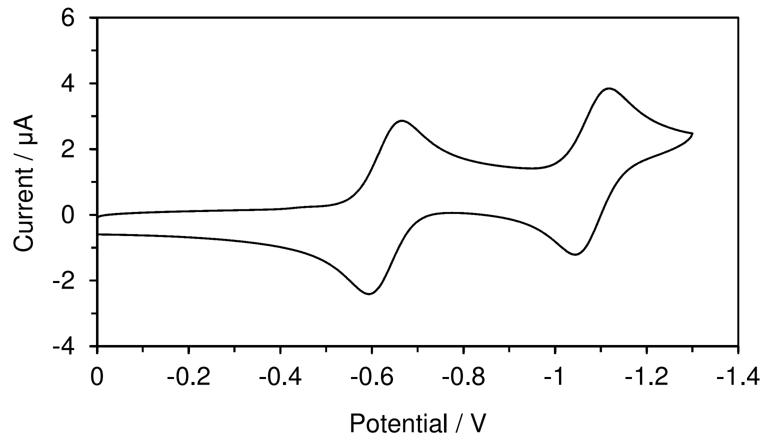

(b)

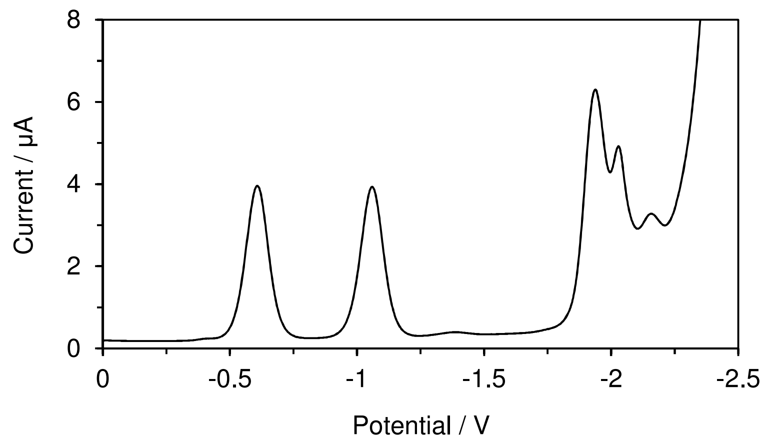

Figure S14. Voltammograms of **8a**$^+$: (a) reduction wave on CV and (b) oxidation wave on DPV in benzonitrile (1 mM) containing Et_4NClO_4 (0.1 M) as a supporting electrolyte; scan rate, 100 mV s^{-1}.

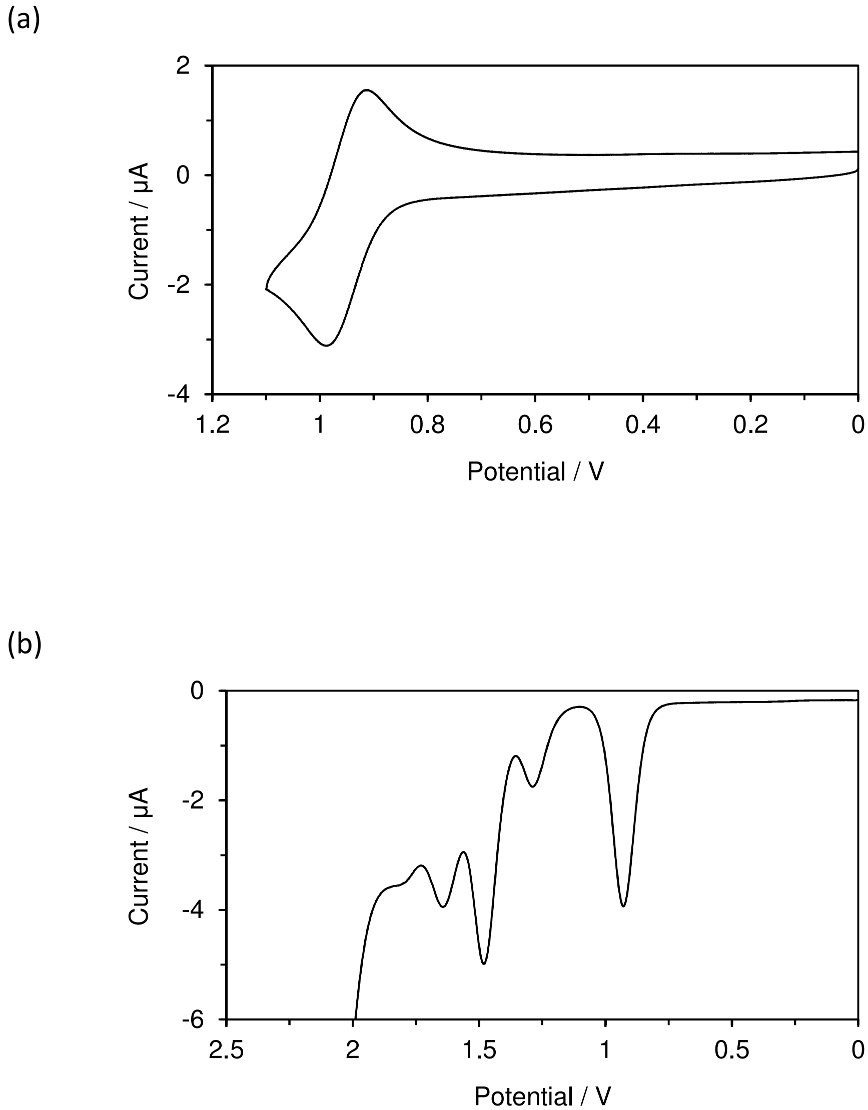

Figure S15. Voltammograms of **8a**$^{+}$: (a) reduction wave on CV and (b) oxidation wave on DPV in benzonitrile (1 mM) containing Et_4NClO_4 (0.1 M) as a supporting electrolyte; scan rate, 100 mV s^{-1}.

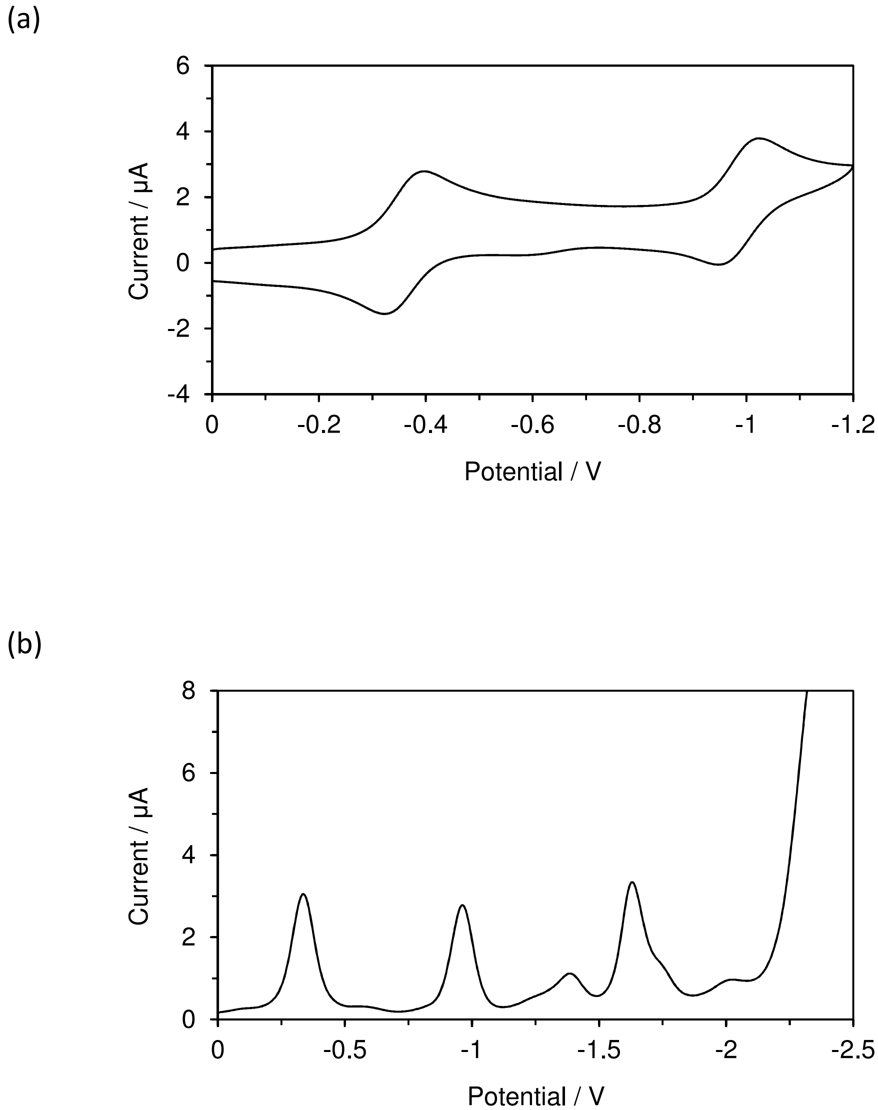

Figure S16. Voltammograms of **8b**$^{+}$: (a) reduction wave on CV and (b) oxidation wave on DPV in benzonitrile (1 mM) containing Et_4NClO_4 (0.1 M) as a supporting electrolyte; scan rate, 100 mV s^{-1}.

(a)

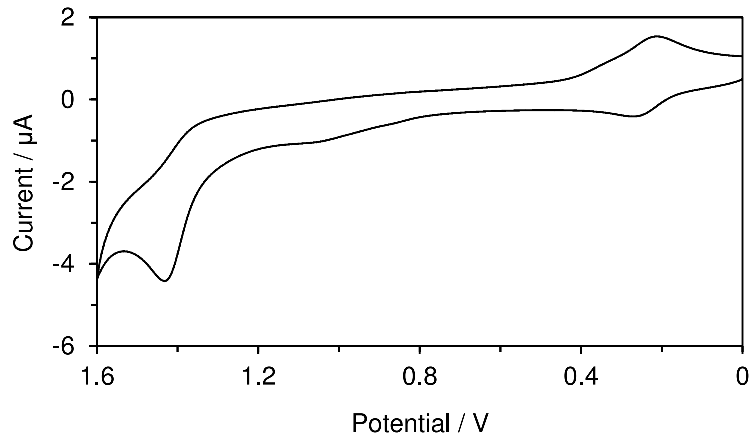

(b)

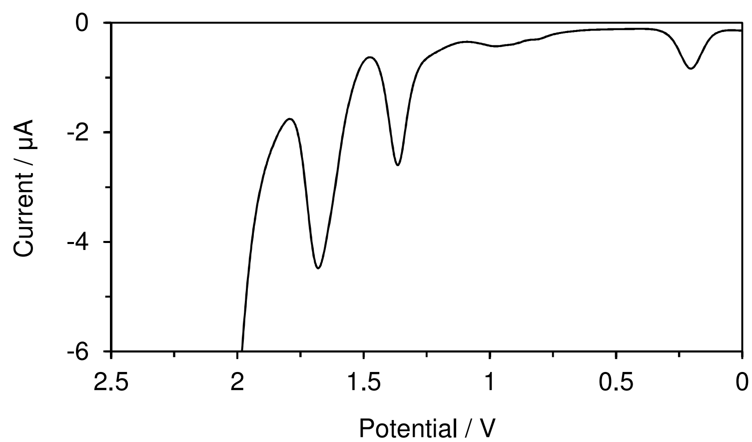

Figure S17. Voltammograms of **8b**$^{+}$: (a) reduction wave on CV and (b) oxidation wave on DPV in benzonitrile (1 mM) containing Et_4NClO_4 (0.1 M) as a supporting electrolyte; scan rate, 100 mV s^{-1}.

(a)

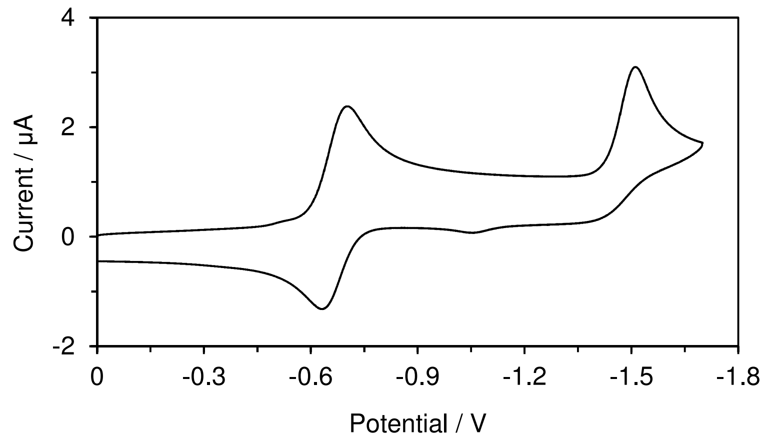

(b)

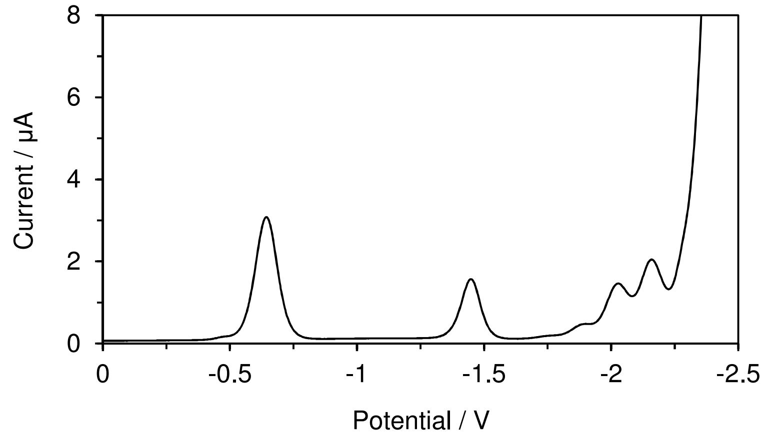

Figure S18. Voltammograms of **11a**$^{+}$: (a) reduction wave on CV and (b) oxidation wave on DPV in benzonitrile (1 mM) containing Et_4NClO_4 (0.1 M) as a supporting electrolyte; scan rate, 100 mV s^{-1}.

(a)

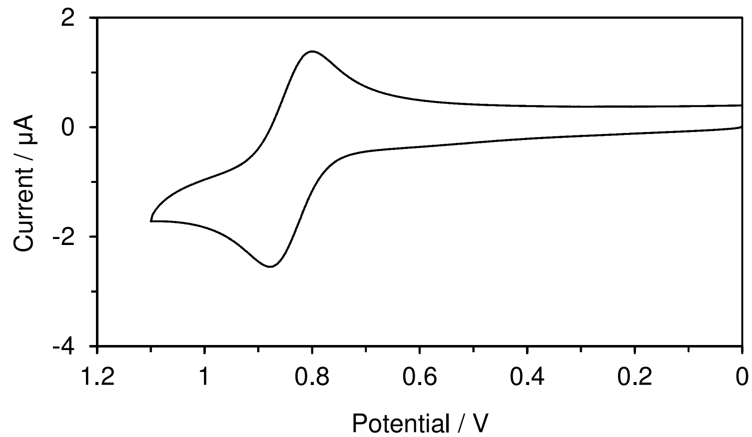

(b)

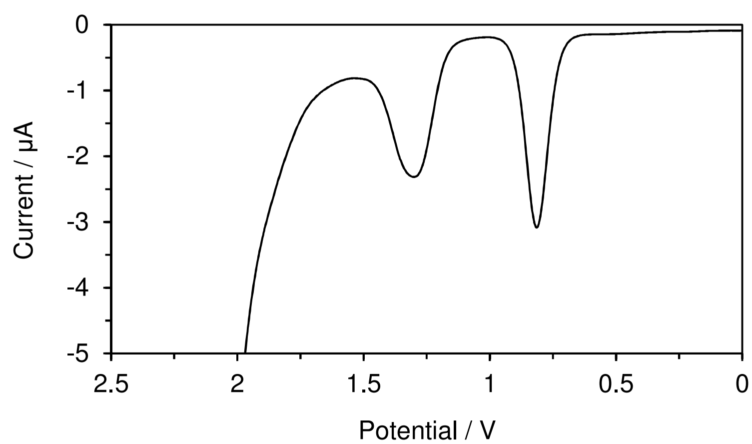

Figure S19. Voltammograms of **11a**$^+$: (a) reduction wave on CV and (b) oxidation wave on DPV in benzonitrile (1 mM) containing Et_4NClO_4 (0.1 M) as a supporting electrolyte; scan rate, 100 mV s^{-1}.

(a)

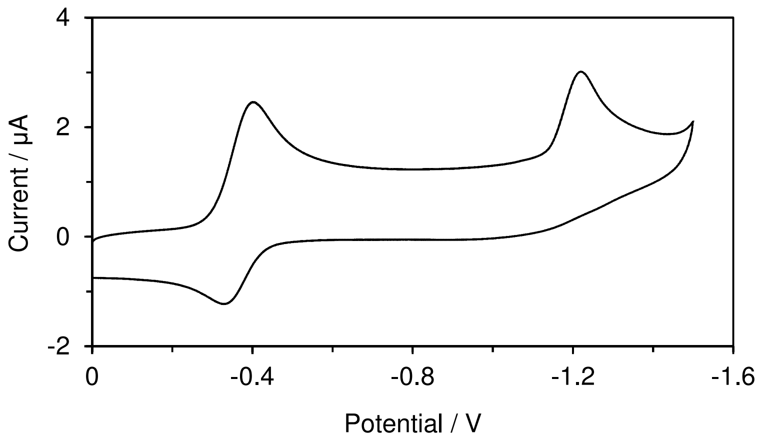

(b)

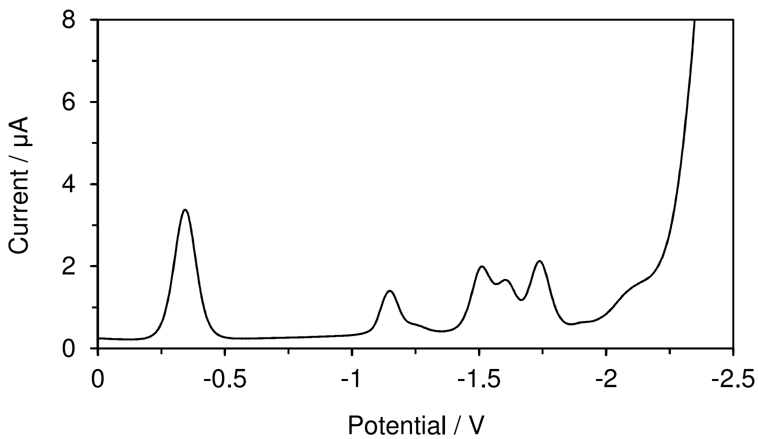

Figure S20. Voltammograms of **11b**$^+$: (a) reduction wave on CV and (b) oxidation wave on DPV in benzonitrile (1 mM) containing Et_4NClO_4 (0.1 M) as a supporting electrolyte; scan rate, 100 mV s^{-1}.

(a)

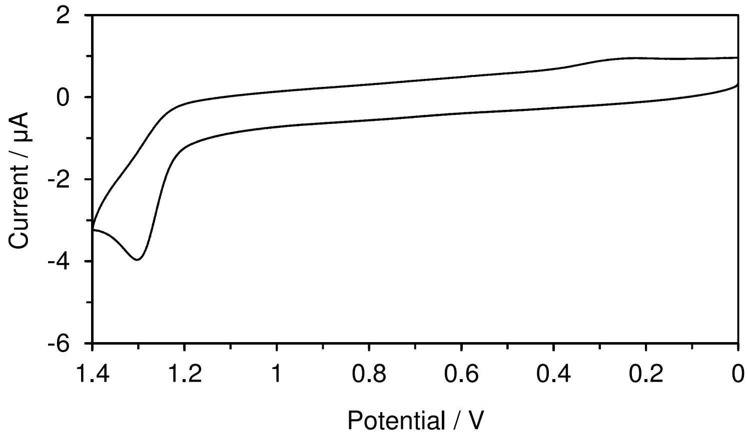

(b)

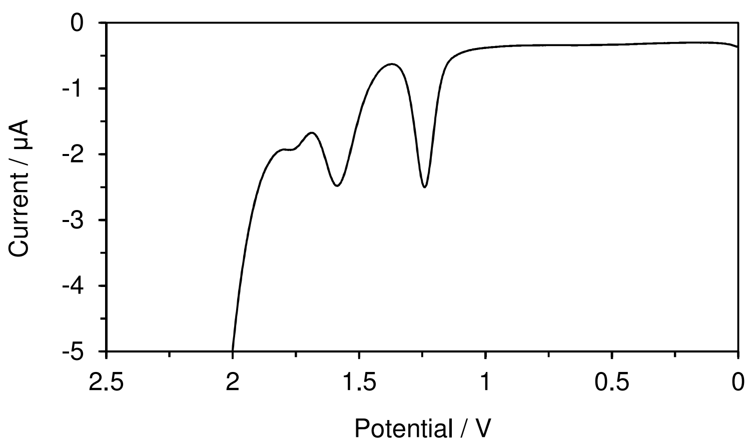

Figure S21. Voltammograms of **11b**$^+$: (a) reduction wave on CV and (b) oxidation wave on DPV in benzonitrile (1 mM) containing Et_4NClO_4 (0.1 M) as a supporting electrolyte; scan rate, 100 mV s^{-1}.

(a)

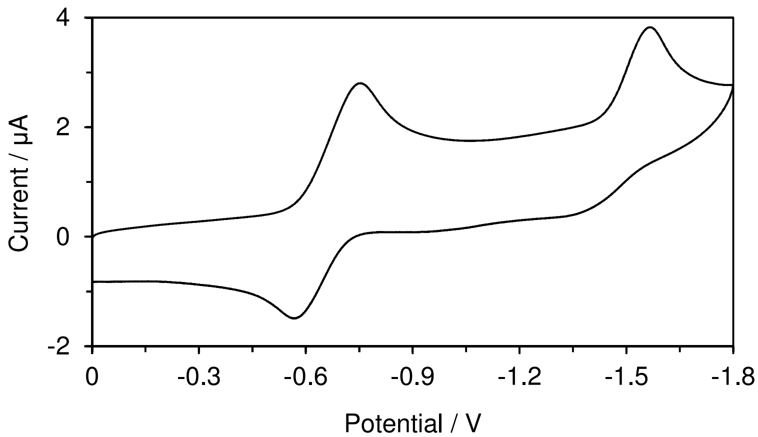

(b)

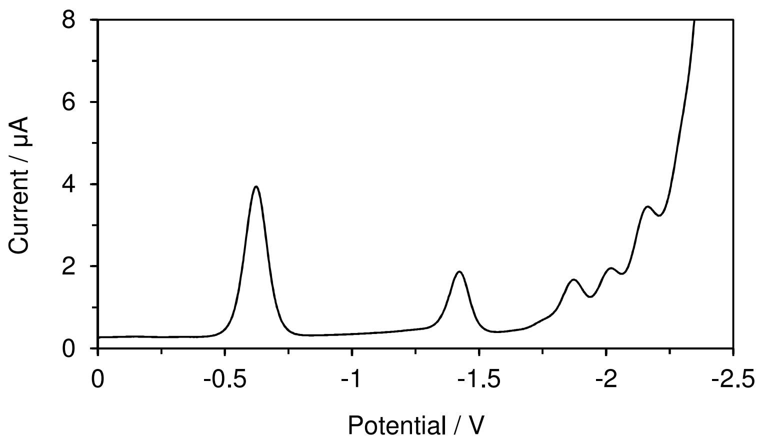

Figure S22. Voltammograms of **11c**$^+$: (a) reduction wave on CV and (b) oxidation wave on DPV in benzonitrile (1 mM) containing Et_4NClO_4 (0.1 M) as a supporting electrolyte; scan rate, 100 mV s^{-1}.

(a)

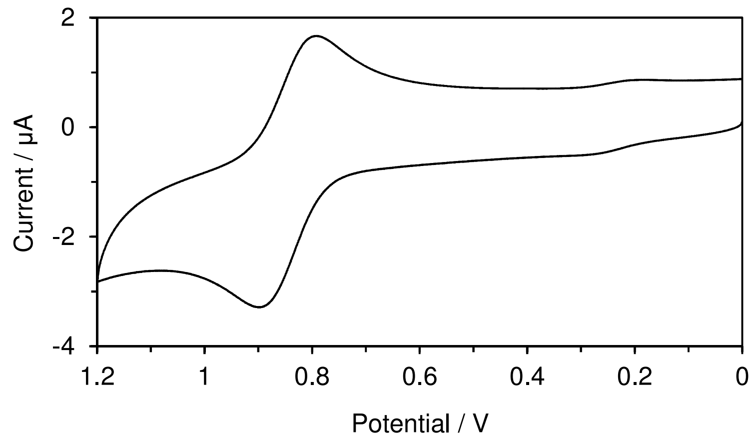

(b)

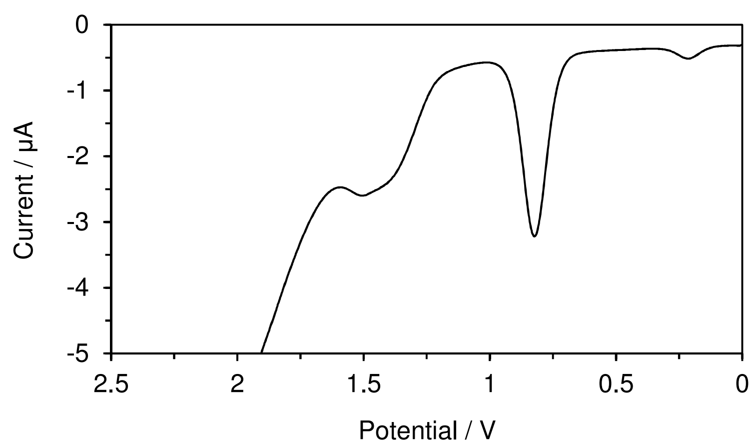

Figure S23. Voltammograms of **11c**$^{+}$: (a) reduction wave on CV and (b) oxidation wave on DPV in benzonitrile (1 mM) containing Et_4NClO_4 (0.1 M) as a supporting electrolyte; scan rate, 100 mV s^{-1}.

(a)

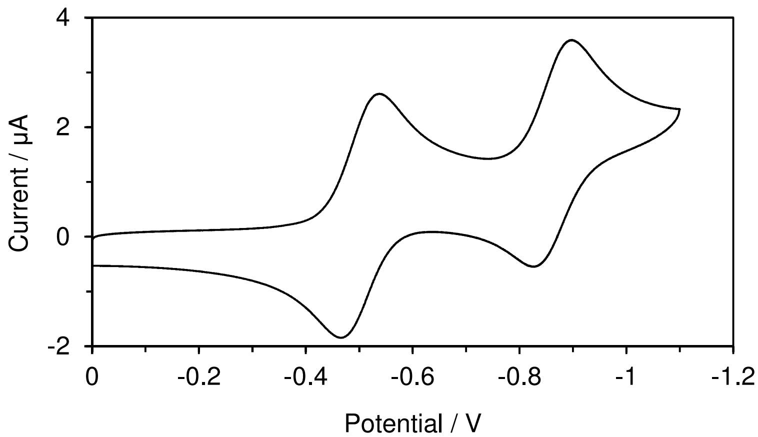

(b)

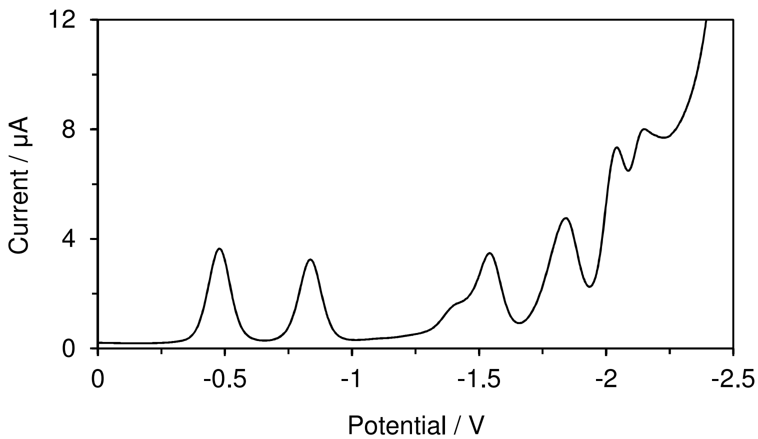

Figure S24. Voltammograms of **11d**$^{+}$: (a) reduction wave on CV and (b) oxidation wave on DPV in benzonitrile (1 mM) containing Et_4NClO_4 (0.1 M) as a supporting electrolyte; scan rate, 100 mV s^{-1}.

(a)

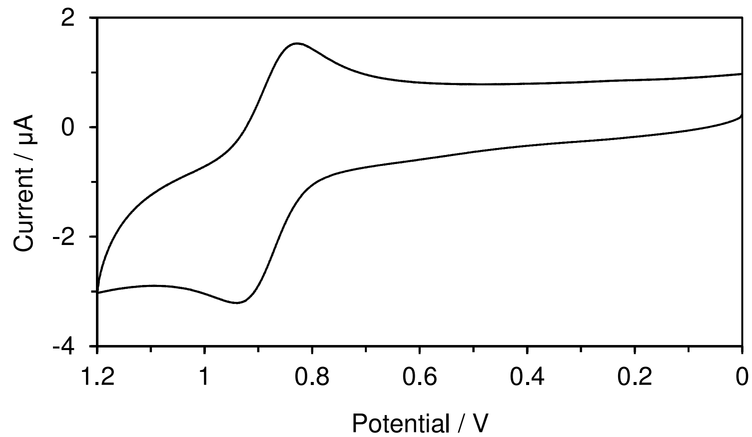

(b)

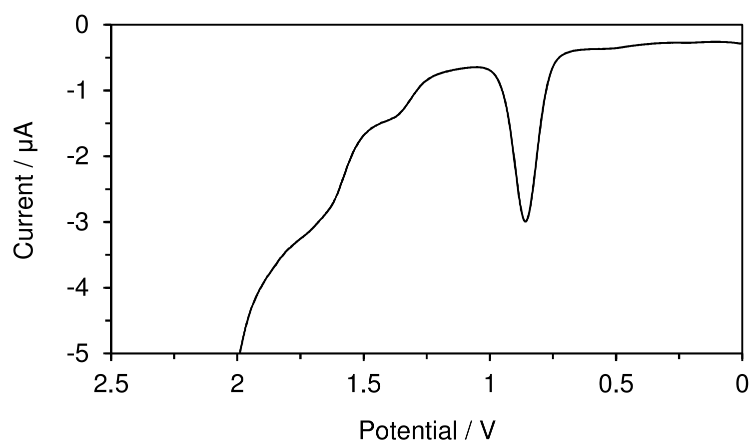

Figure S25. Voltammograms of **11d**$^{+}$: (a) reduction wave on CV and (b) oxidation wave on DPV in benzonitrile (1 mM) containing Et_4NClO_4 (0.1 M) as a supporting electrolyte; scan rate, 100 mV s^{-1}.

(a)

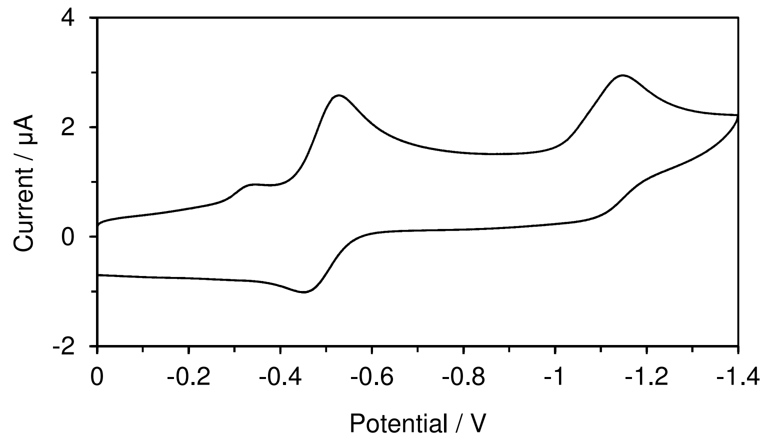

(b)

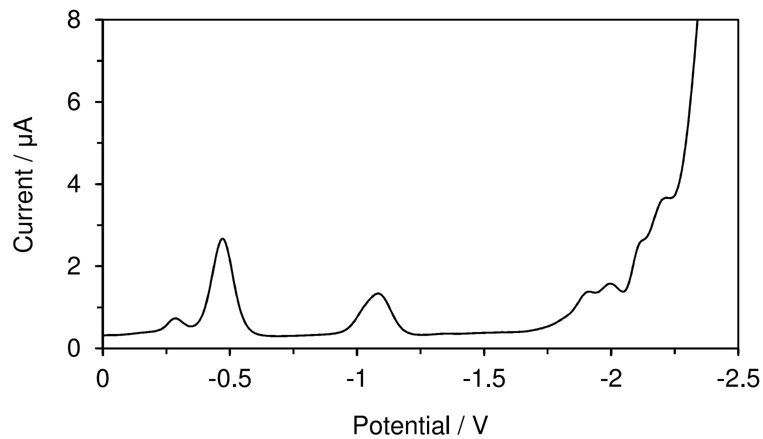

Figure S26. Voltammograms of **14**$^{+}$: (a) reduction wave on CV and (b) oxidation wave on DPV in benzonitrile (1 mM) containing Et_4NClO_4 (0.1 M) as a supporting electrolyte; scan rate, 100 mV s^{-1}.

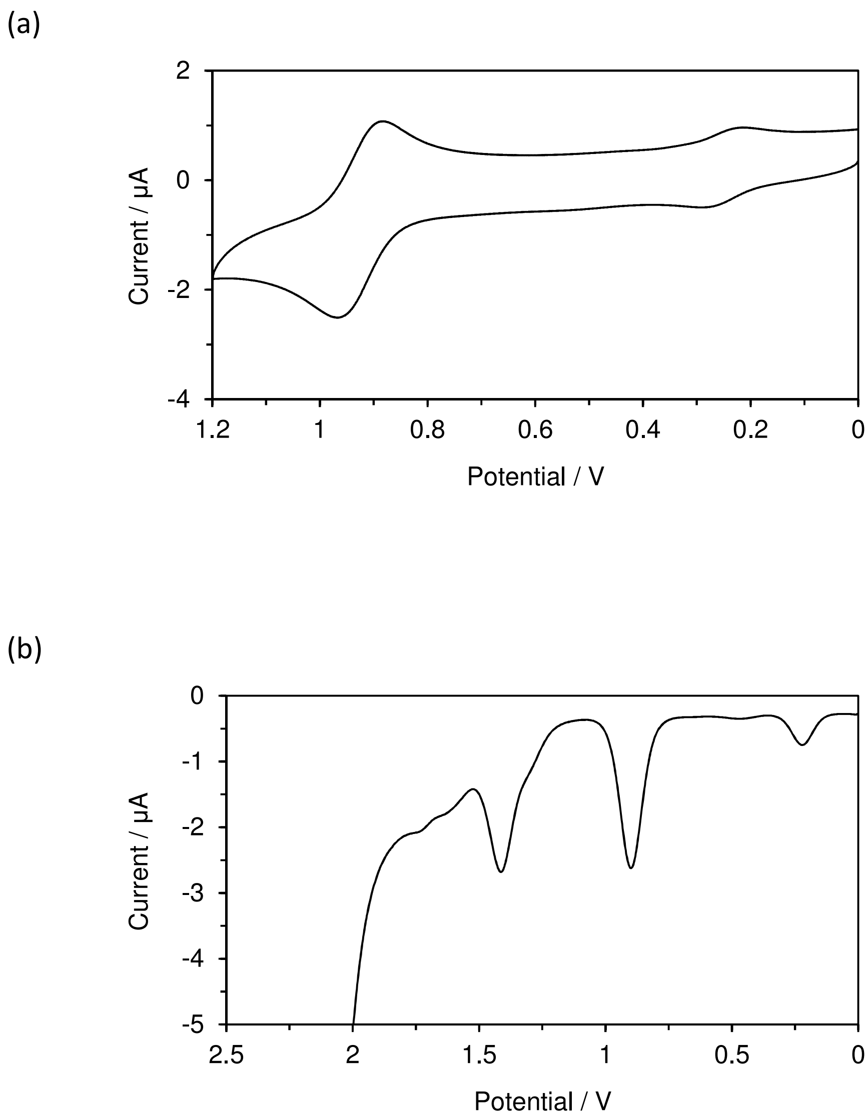

Figure S27. Voltammograms of **14**$^+$: (a) reduction wave on CV and (b) oxidation wave on DPV in benzonitrile (1 mM) containing Et_4NClO_4 (0.1 M) as a supporting electrolyte; scan rate, 100 mV s^{-1}.

4. Spectroelectrograms of 5a$^+$, 5b$^+$, 8a$^+$, 8b$^+$, 11a–d$^+$, and 14$^+$

(a)

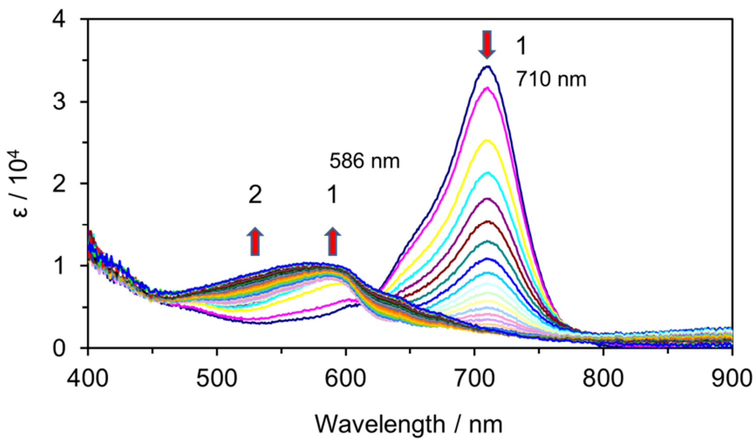

(b)

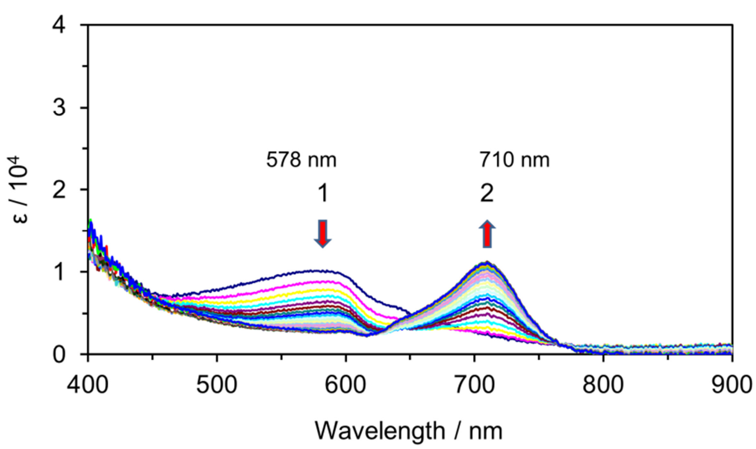

Figure S28. Continuous change in the visible spectrum of **5a**$^+$: (a) constant-current electrochemical reduction (70 μA) and (b) reverse oxidation of the reduced species (70 μA) in benzonitrile (2.5 × 10^{-4} M, 2 mL) containing Et_4NClO_4 (0.1 M) at 1 min intervals.

(a)

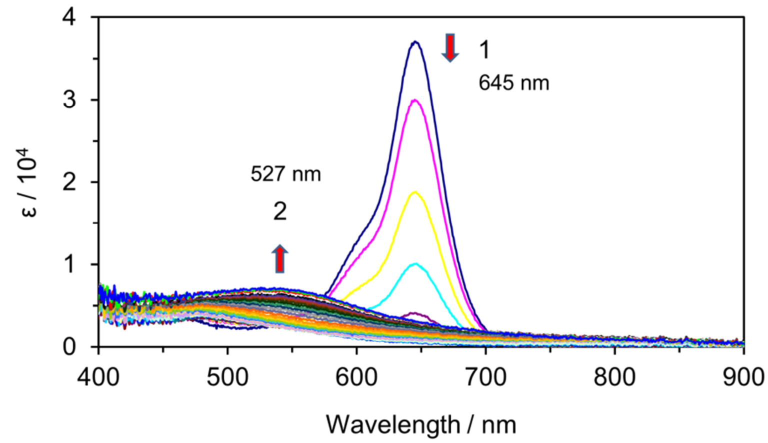

(b)

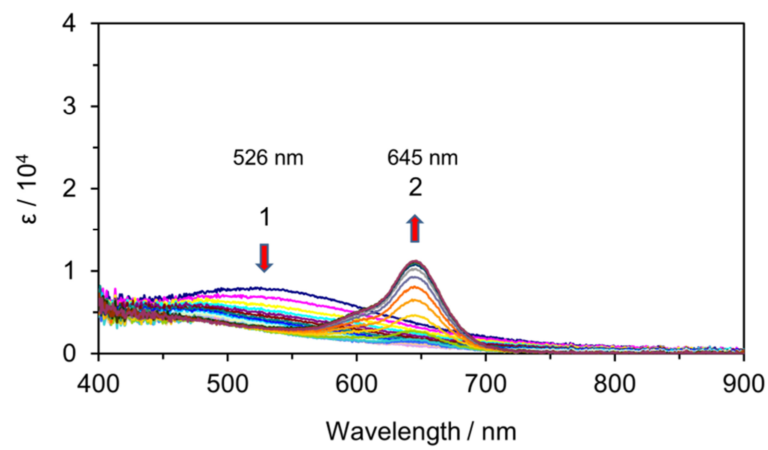

Figure S29. Continuous change in the visible spectrum of **5b**$^{+}$: (a) constant-current electrochemical reduction (70 μA) and (b) reverse oxidation of the reduced species (70 μA) in benzonitrile (2.6×10^{-4} M, 2 mL) containing Et_4NClO_4 (0.1 M) at 1 min intervals.

(a)

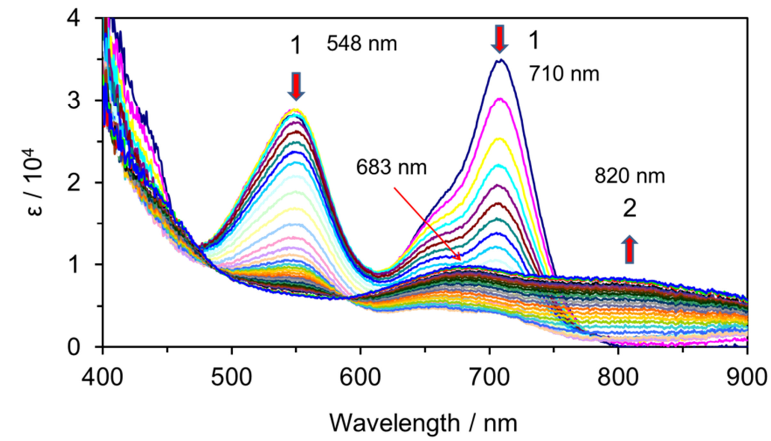

(b)

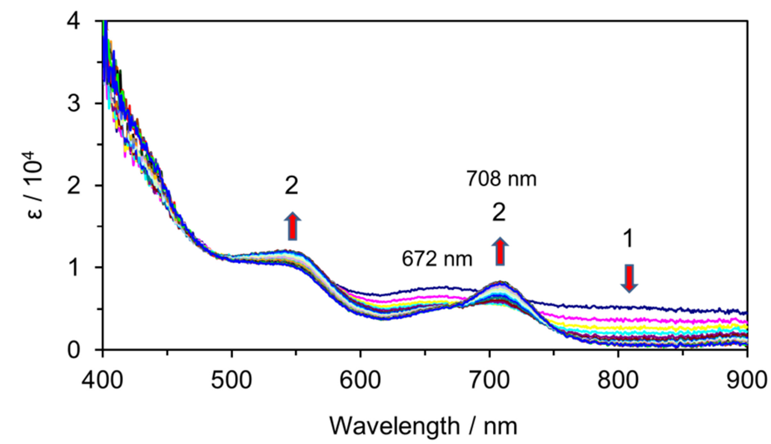

Figure S30. Continuous change in the visible spectrum of **8a**$^{+}$: (a) constant-current electrochemical reduction (70 uA) and (b) reverse oxidation of the reduced species (70 uA) in benzonitrile (2.2×10^{-4} M, 2 mL) containing Et_4NClO_4 (0.1 M) at 1 min intervals.

(a)

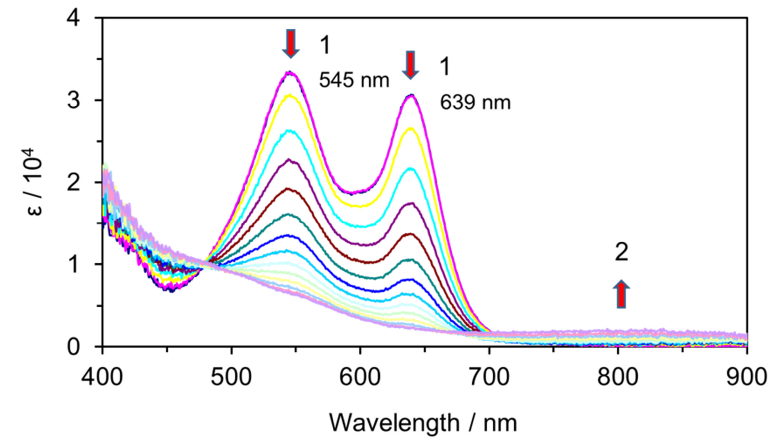

(b)

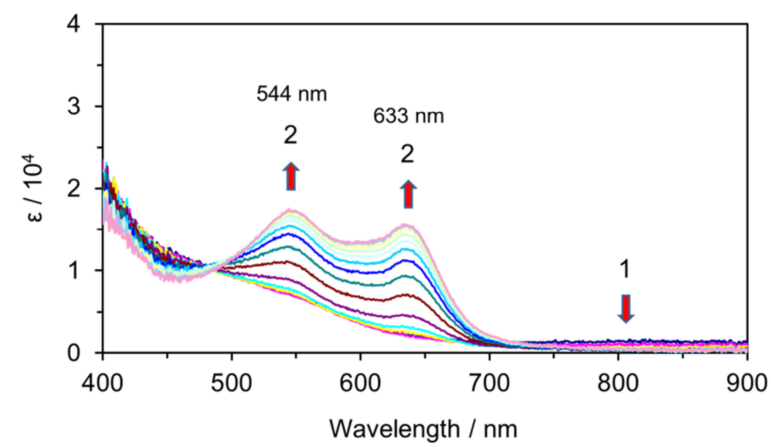

Figure S31. Continuous change in the visible spectrum of **8b**$^+$: (a) constant-current electrochemical reduction (60 uA) and (b) reverse oxidation of the reduced species (60 uA) in benzonitrile (2.7×10^{-5} M, 2 mL) containing Et_4NClO_4 (0.1 M) at 1 min intervals.

(a)

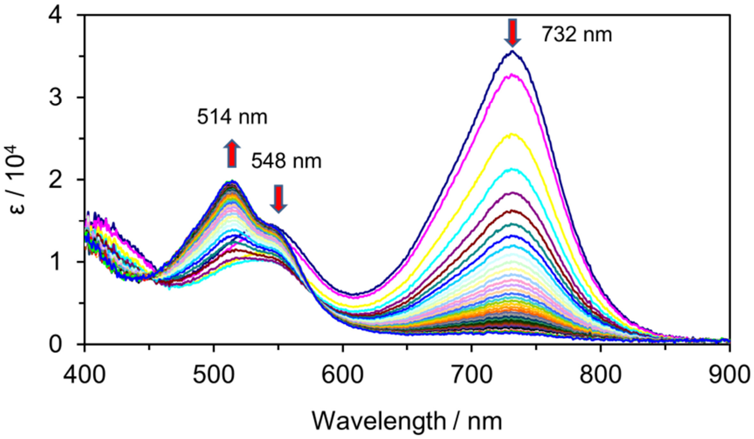

(b)

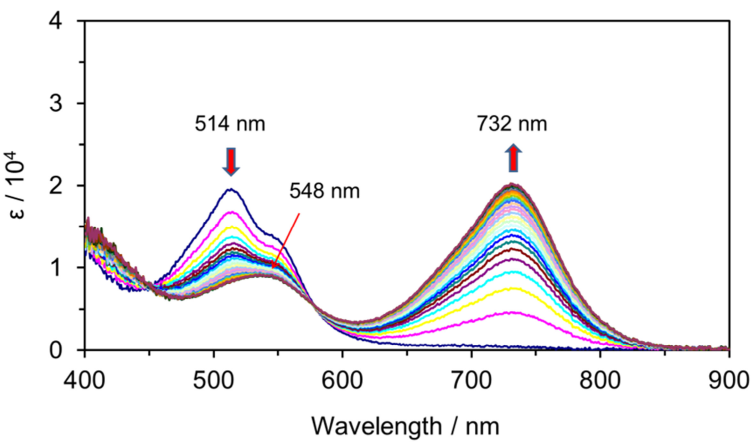

Figure S32. Continuous change in the visible spectrum of **11a**$^{+}$: (a) constant-current electrochemical reduction (70 uA) and (b) reverse oxidation of the reduced species (70 uA) in benzonitrile (2.9×10^{-4} M, 2 mL) containing Et_4NClO_4 (0.1 M) at 1 min intervals.

(a)

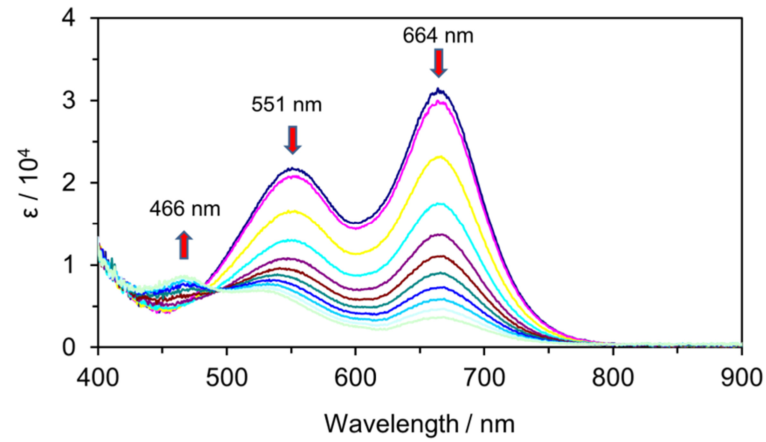

(b)

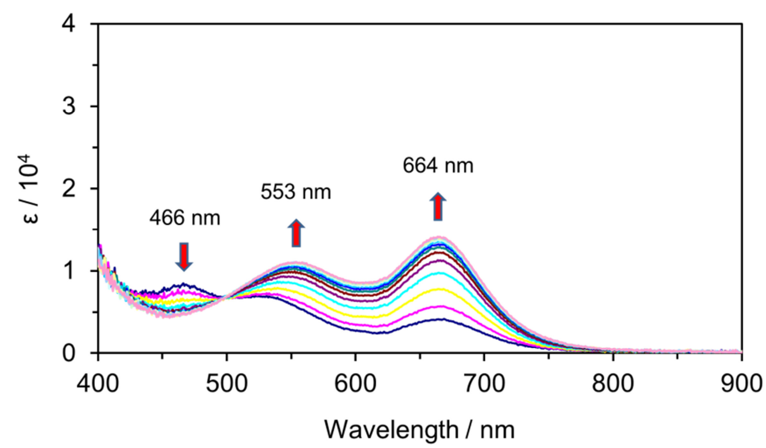

Figure S33. Continuous change in the visible spectrum of **11b**$^{+}$: (a) constant-current electrochemical reduction (70 uA) and (b) reverse oxidation of the reduced species (70 uA) in benzonitrile (4.1×10^{-5} M, 2 mL) containing Et_4NClO_4 (0.1 M) at 1 min intervals.

(a)

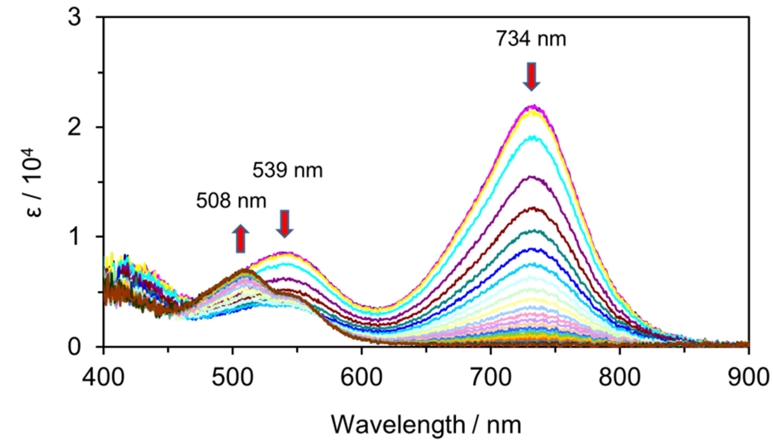

(b)

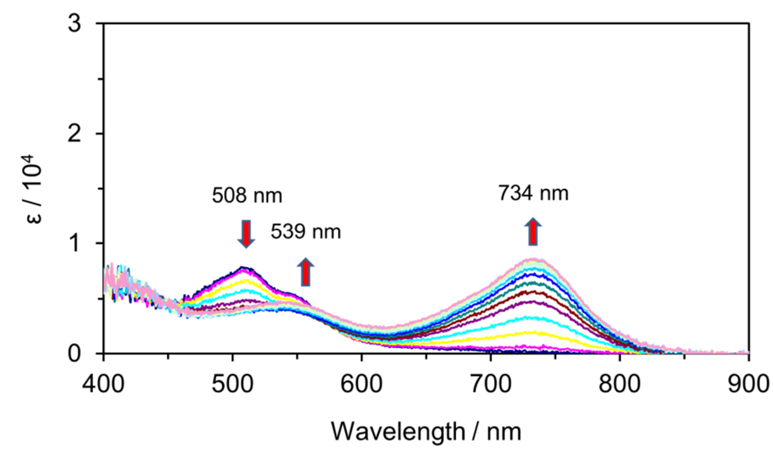

Figure S34. Continuous change in the visible spectrum of **11c**$^{+}$: (a) constant-current electrochemical reduction (70 μA) and (b) reverse oxidation of the reduced species (70 μA) in benzonitrile (2.7×10^{-4} M, 2 mL) containing Et_4NClO_4 (0.1 M) at 1 min intervals.

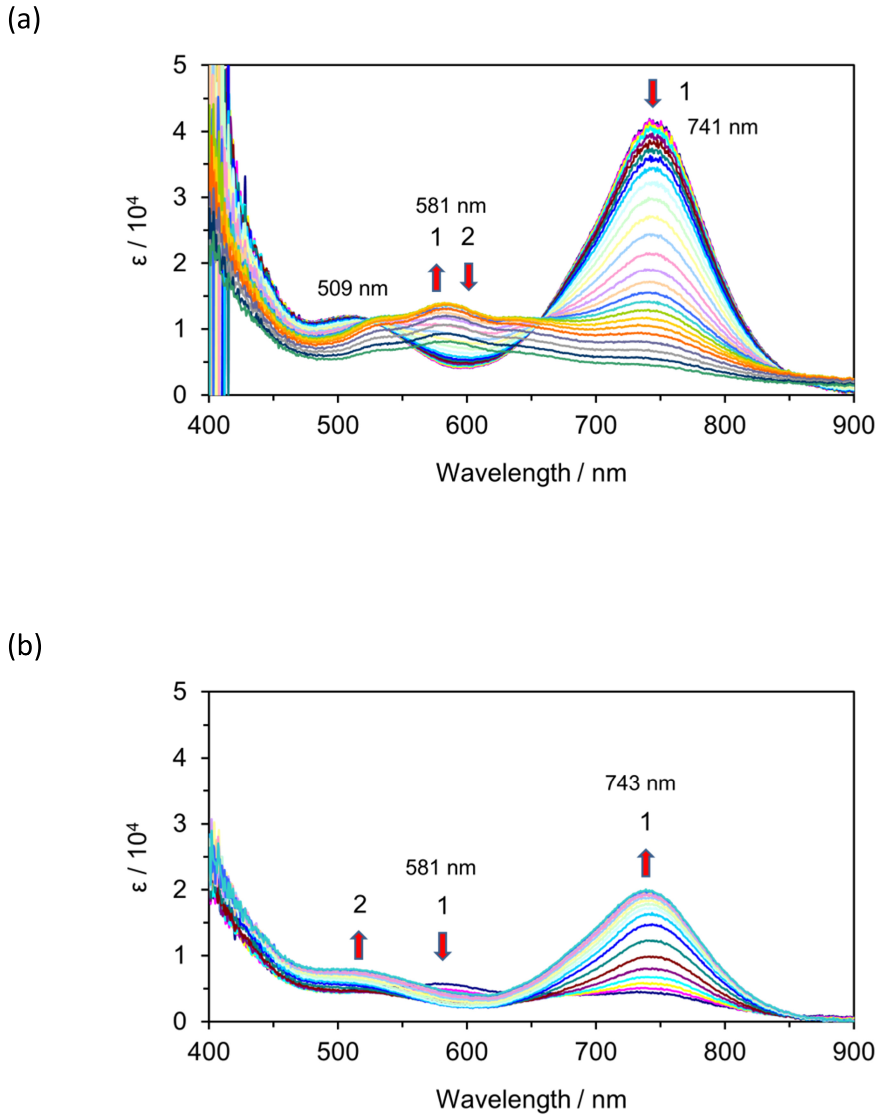

Figure S35. Continuous change in the visible spectrum of **11d**$^+$: (a) constant-current electrochemical reduction (30 μA) and (b) reverse oxidation of the reduced species (30 μA) in benzonitrile (4.1×10^{-4} M, 2 mL) containing Et_4NClO_4 (0.1 M) at 1 min intervals.

(a)

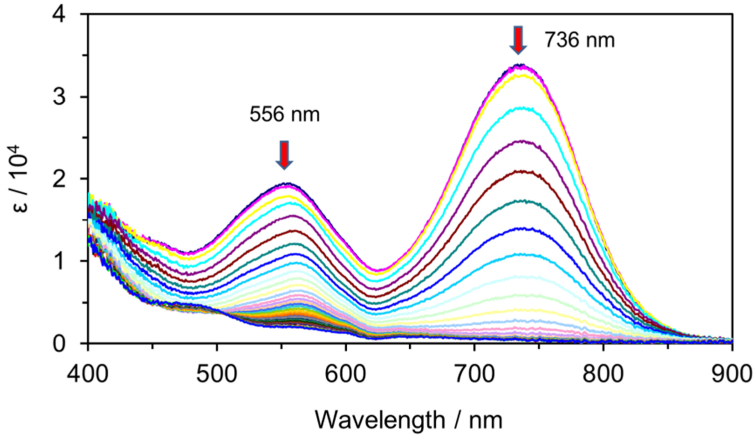

(b)

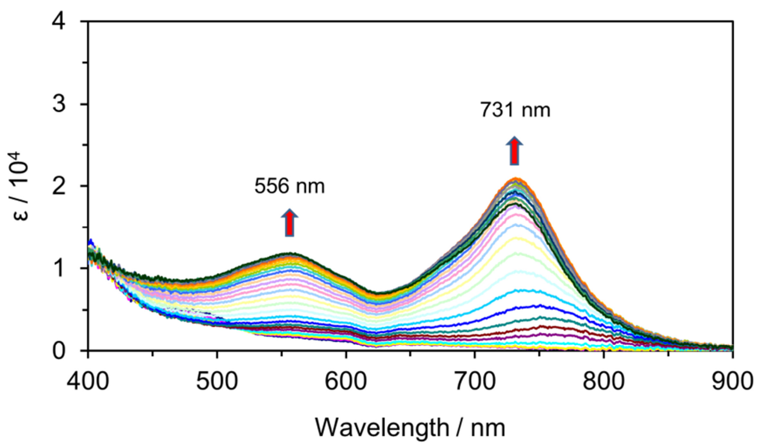

Figure S36. Continuous change in the visible spectrum of **14**$^{+}$: (a) constant-current electrochemical reduction (70 µA) and (b) reverse oxidation of the reduced species (70 µA) in benzonitrile (3.9×10^{-4} M, 2 mL) containing Et_4NClO_4 (0.1 M) at 1 min intervals.

5. Copies of ^{1}H and ^{13}C NMR spectra of reported compounds

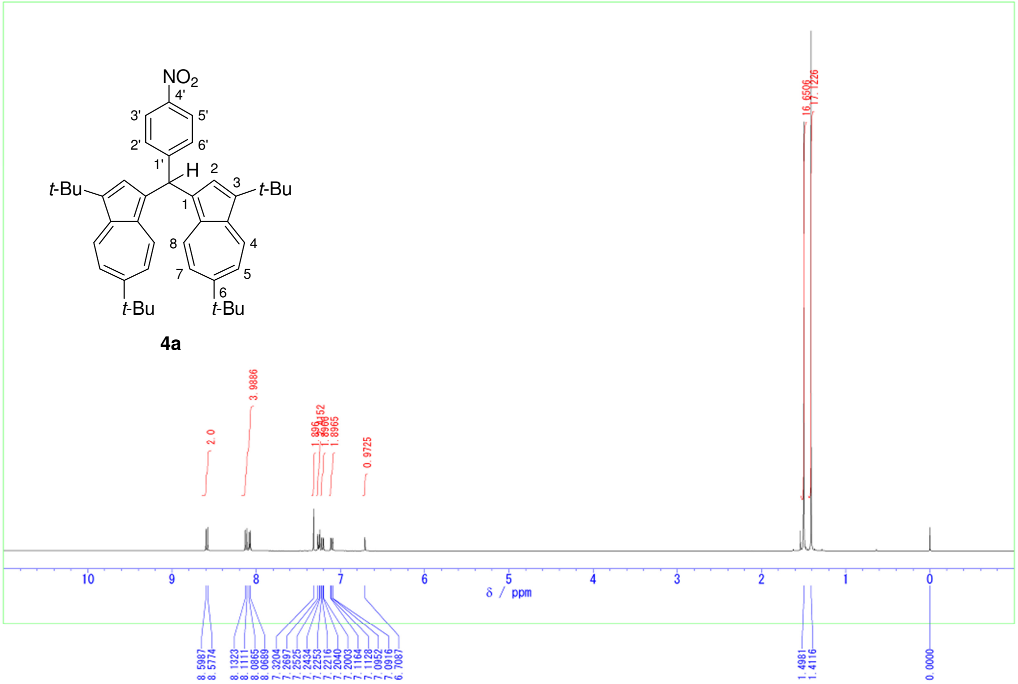

Figure S37. ^{1}H NMR spectrum (500 MHz) of bis(3,6-di-*tert*-butyl-1-azulenyl)(4-nitrophenyl)methane (**4a**) in $CDCl_3$.

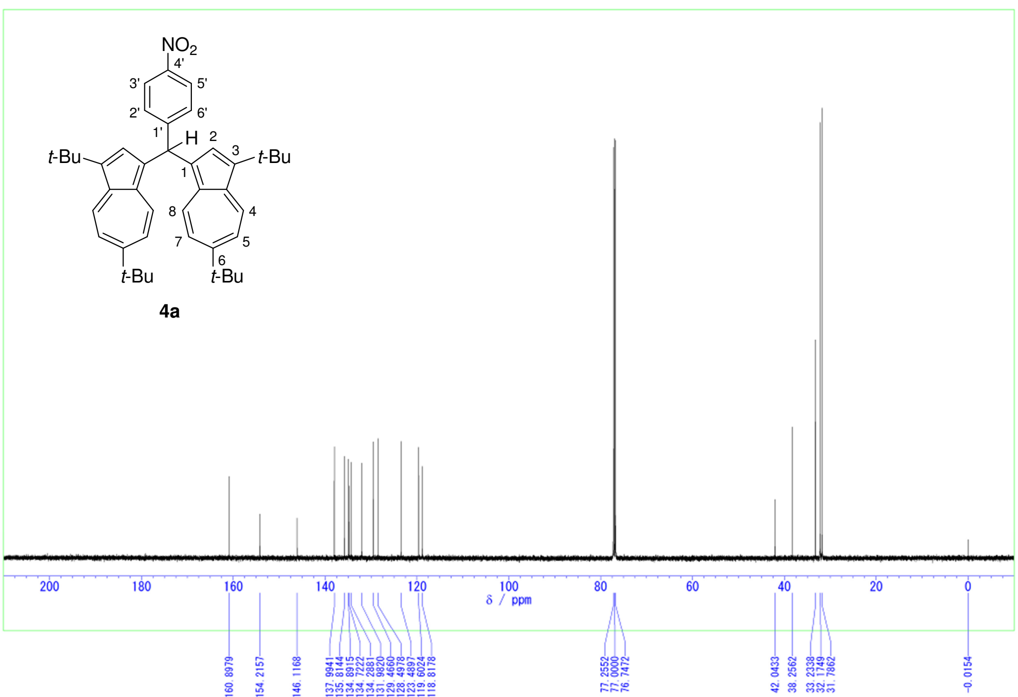

Figure S38. ^{13}C NMR spectrum (125 MHz) of bis(3,6-di-*tert*-butyl-1-azulenyl)(4-nitrophenyl)methane (**4a**) in $CDCl_3$.

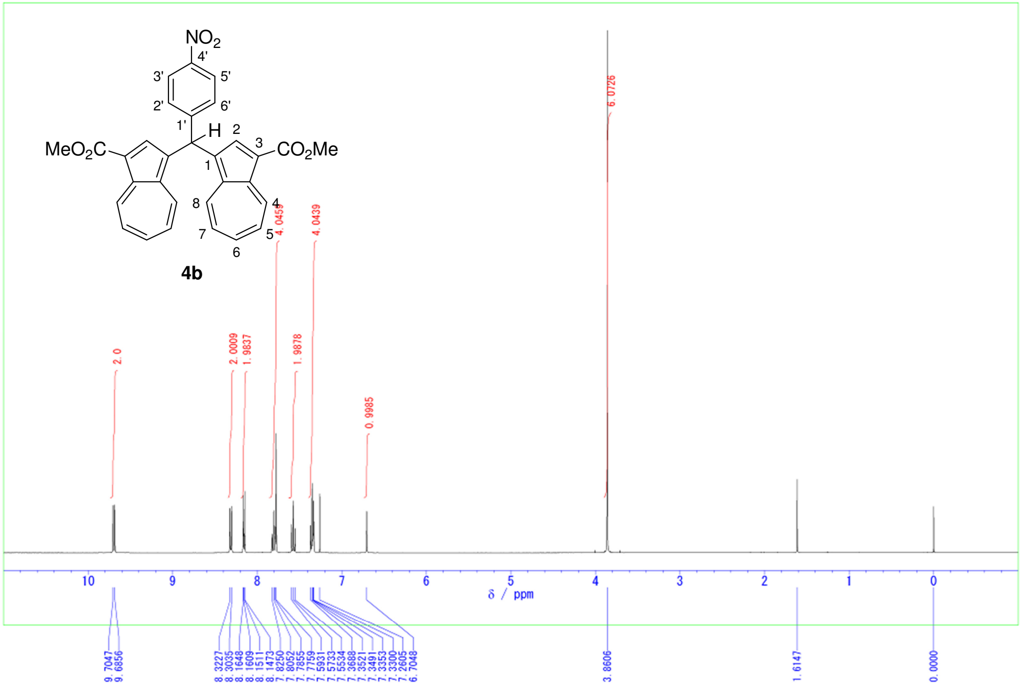

Figure S39. ^{1}H NMR spectrum (500 MHz) of bis(3-methoxycarbonyl-1-azulenyl)(4-nitrophenyl)methane (**4b**) in $CDCl_3$.

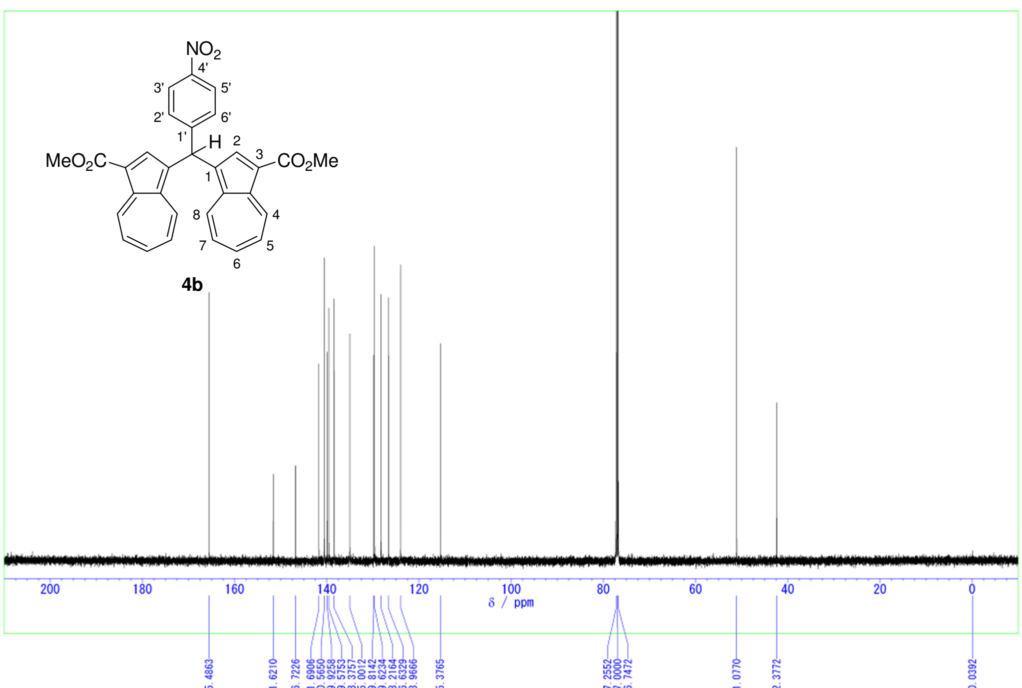

Figure S40. ^{13}C NMR spectrum (125 MHz) of bis(3-methoxycarbonyl-1-azulenyl)(4-nitrophenyl)methane (**4b**) in $CDCl_3$.

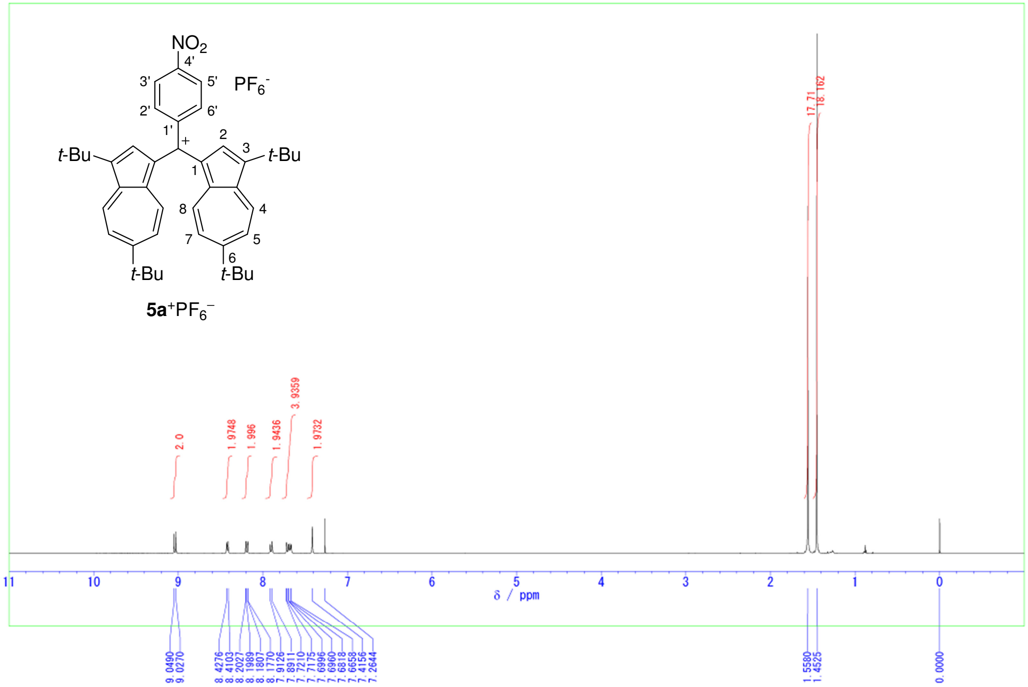

Figure S41. ^{1}H NMR spectrum (500 MHz) of bis(3,6-di-*tert*-butyl-1-azulenyl)(4-nitrophenyl)methylium hexafluorophosphate (**5a**$^{+}$$PF_6^{-}$) in $CDCl_3$ at room temperature.

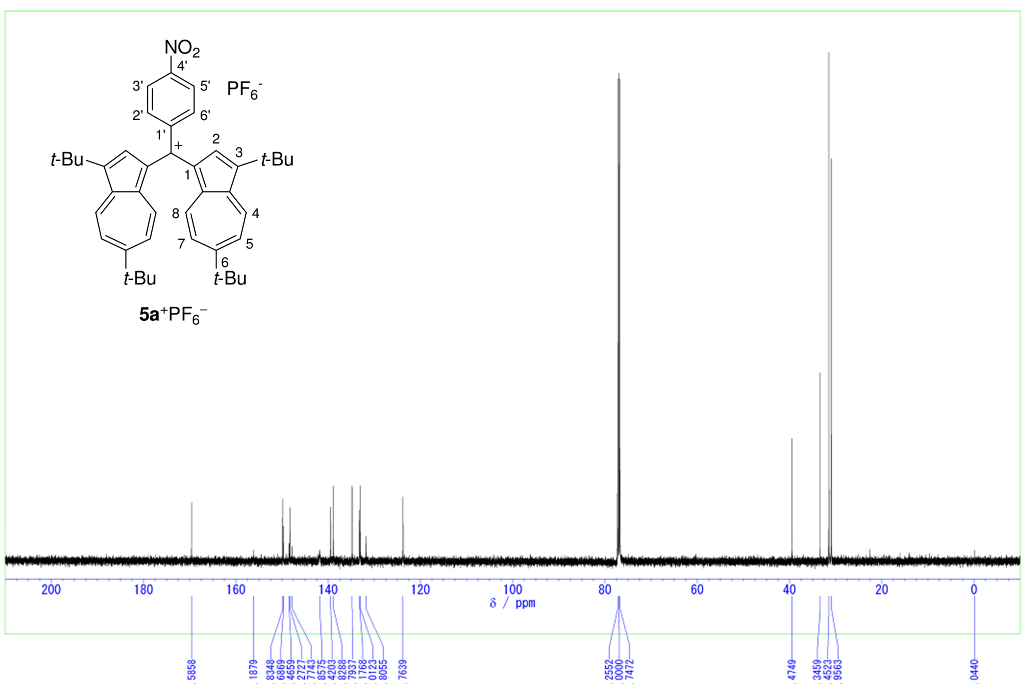

Figure S42. ^{13}C NMR spectrum (125 MHz) of bis(3,6-di-*tert*-butyl-1-azulenyl)(4-nitrophenyl)methylium hexafluorophosphate (**5a**$^{+}$$PF_6^{-}$) in $CDCl_3$ at room temperature.

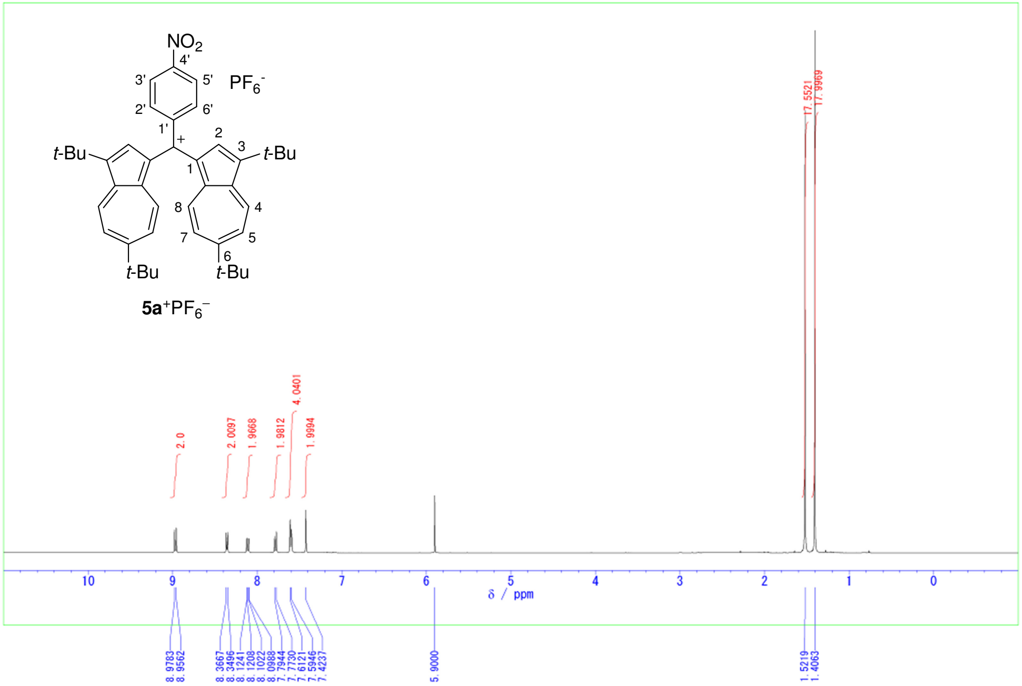

Figure S43. ^{1}H NMR spectrum (500 MHz) of bis(3,6-di-*tert*-butyl-1-azulenyl)(4-nitrophenyl)methylium hexafluorophosphate (**5a**$^{+}PF_6^{-}$) in $(CDCl_2)_2$ at 80 °C.

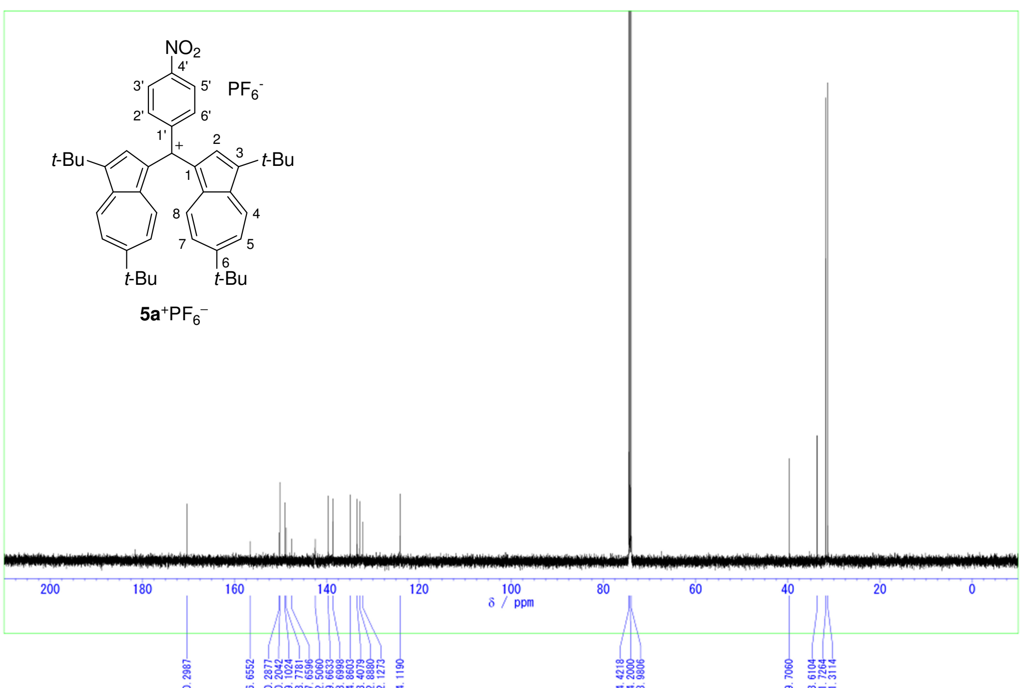

Figure S44. ^{13}C NMR spectrum (125 MHz) of bis(3,6-di-*tert*-butyl-1-azulenyl)(4-nitrophenyl)methylium hexafluorophosphate (**5a**$^{+}PF_6^{-}$) in $(CDCl_2)_2$ at 80 °C.

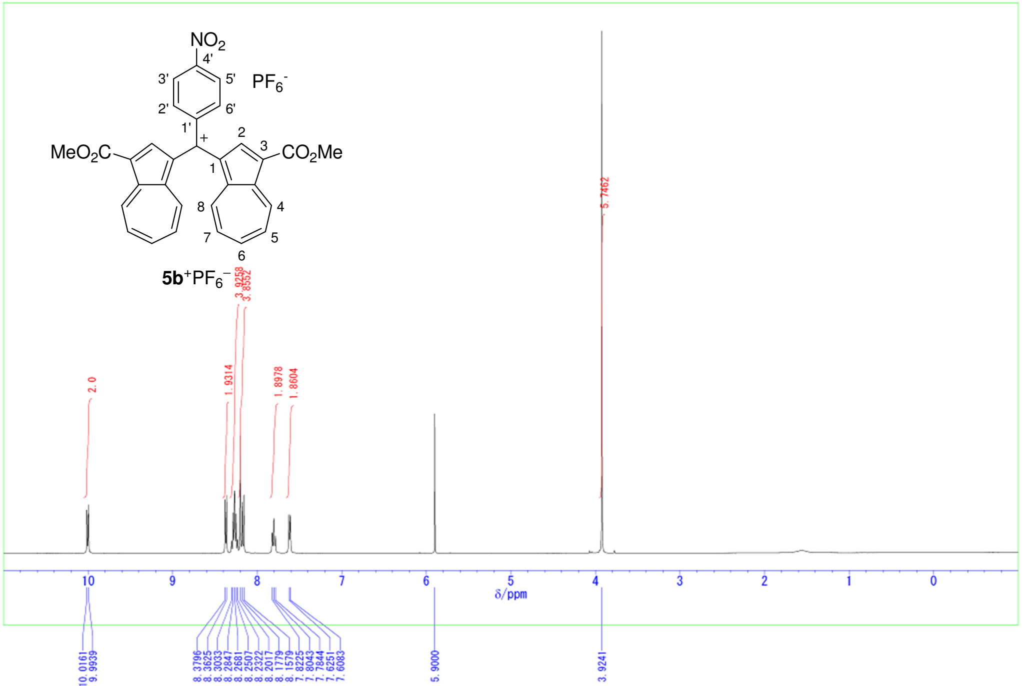

Figure S45. ^{1}H NMR spectrum (500 MHz) of bis(3-methoxycarbonyl-1-azulenyl)(4-nitrophenyl)methylium hexafluorophosphate (**5b**$^{+}PF_6^{-}$) in $(CDCl_2)_2$ at 80 °C.

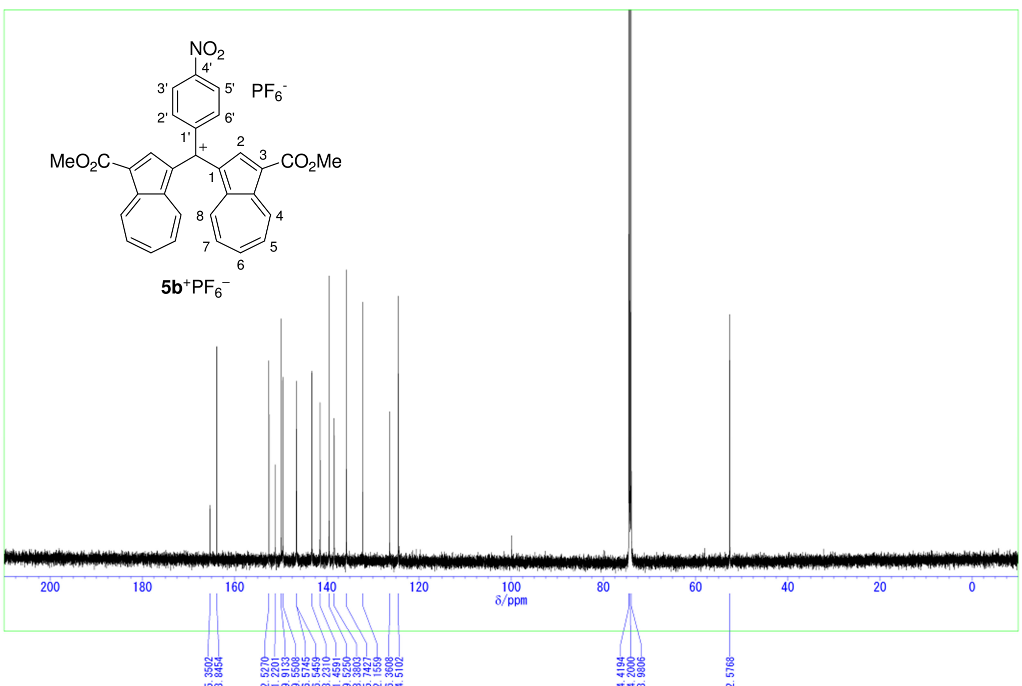

Figure S46. ^{13}C NMR spectrum (125 MHz) of bis(3-methoxycarbonyl-1-azulenyl)(4-nitrophenyl)methylium hexafluorophosphate (**5b**$^{+}PF_6^{-}$) in $(CDCl_2)_2$ at 80 °C.

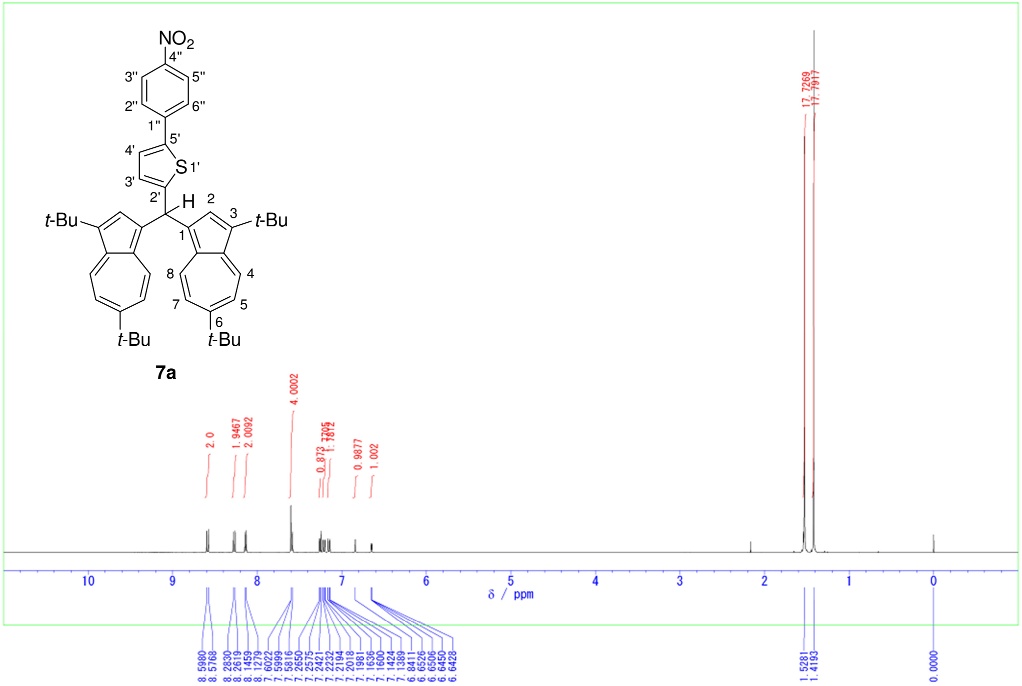

Figure S47. ^{1}H NMR spectrum (500 MHz) of bis(3,6-di-*tert*-butyl-1-azulenyl)[5-(4-nitrophenyl)-2-thienyl]methane (**7a**) in $CDCl_3$.

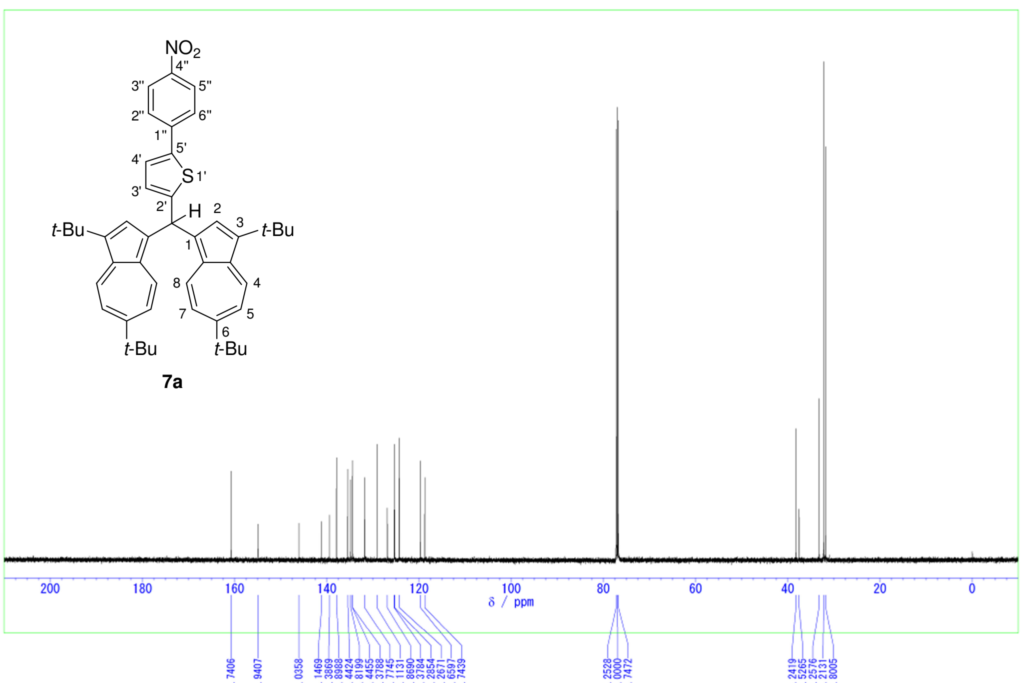

Figure S48. ^{13}C NMR spectrum (125 MHz) of bis(3,6-di-*tert*-butyl-1-azulenyl)[5-(4-nitrophenyl)-2-thienyl]methane (**7a**) in $CDCl_3$.

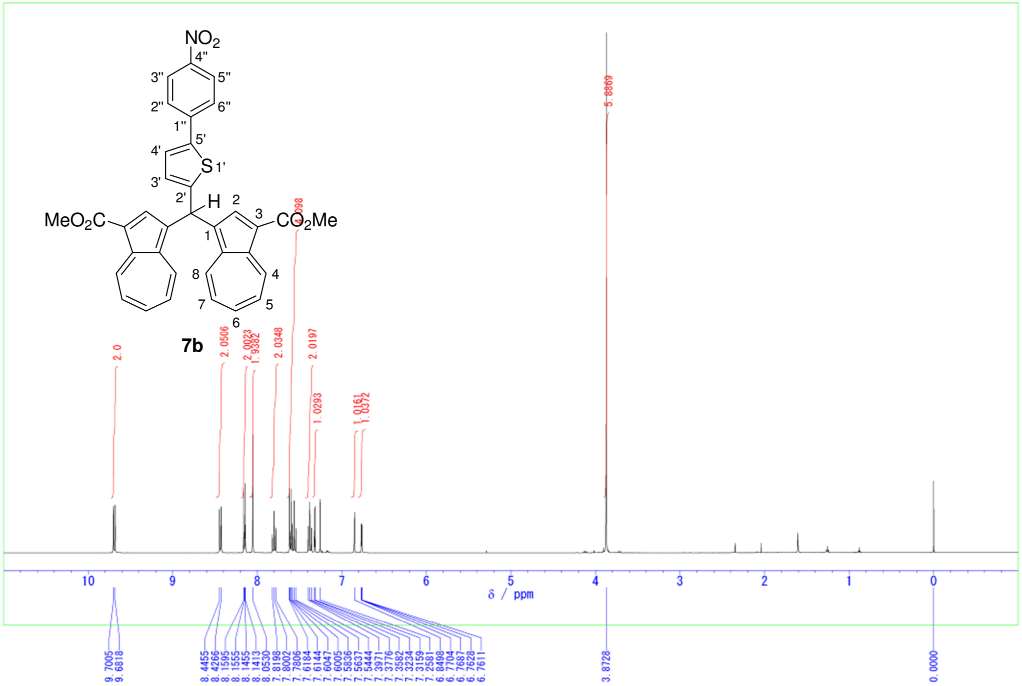

Figure S49. ^{1}H NMR spectrum (500 MHz) of bis(3-methoxycarbonyl-1-azulenyl)[5-(4-nitrophenyl)-2-thienyl]methane (**7b**) in $CDCl_3$.

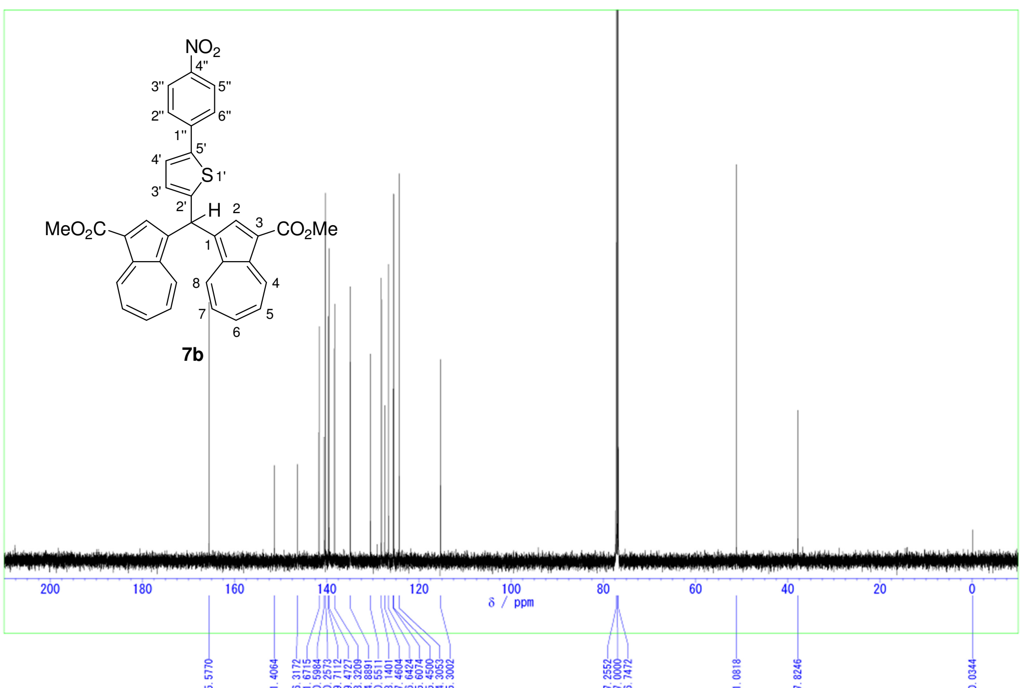

Figure S50. ^{13}C NMR spectrum (125 MHz) of bis(3-methoxycarbonyl-1-azulenyl)[5-(4-nitrophenyl)-2-thienyl]methane (**7b**) in $CDCl_3$.

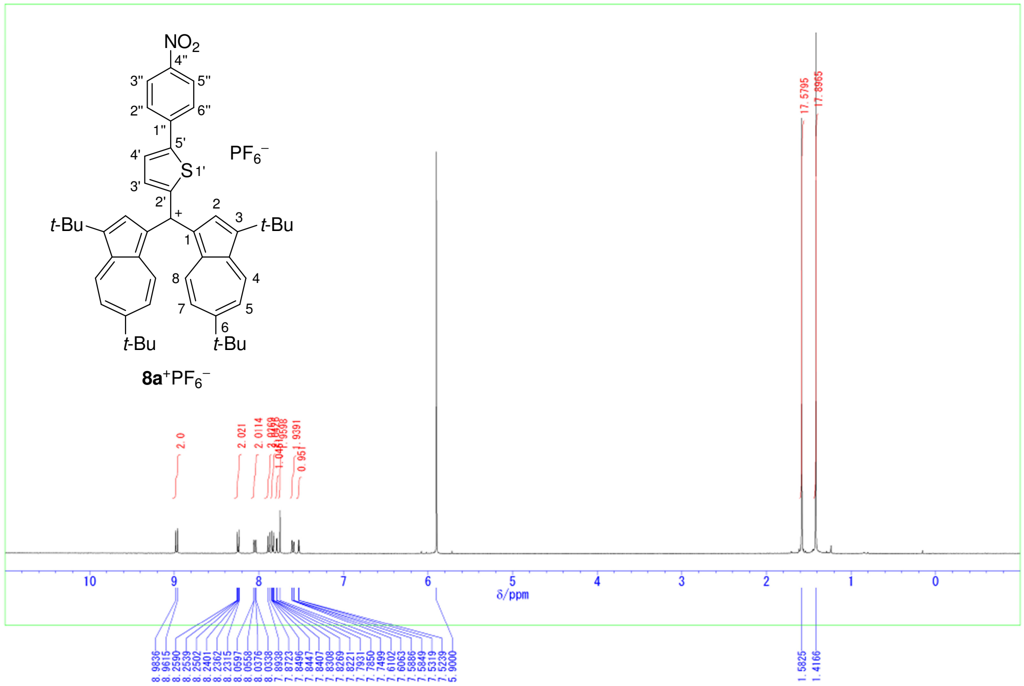

Figure S51. ^{1}H NMR spectrum (600 MHz) of bis(3,6-di-*tert*-butyl-1-azulenyl)[5-(4-nitrophenyl)-2-thienyl]methylium hexafluorophosphate ($\mathbf{8a}^{+}PF_6^{-}$) in $(CDCl_2)_2$ at 100 °C.

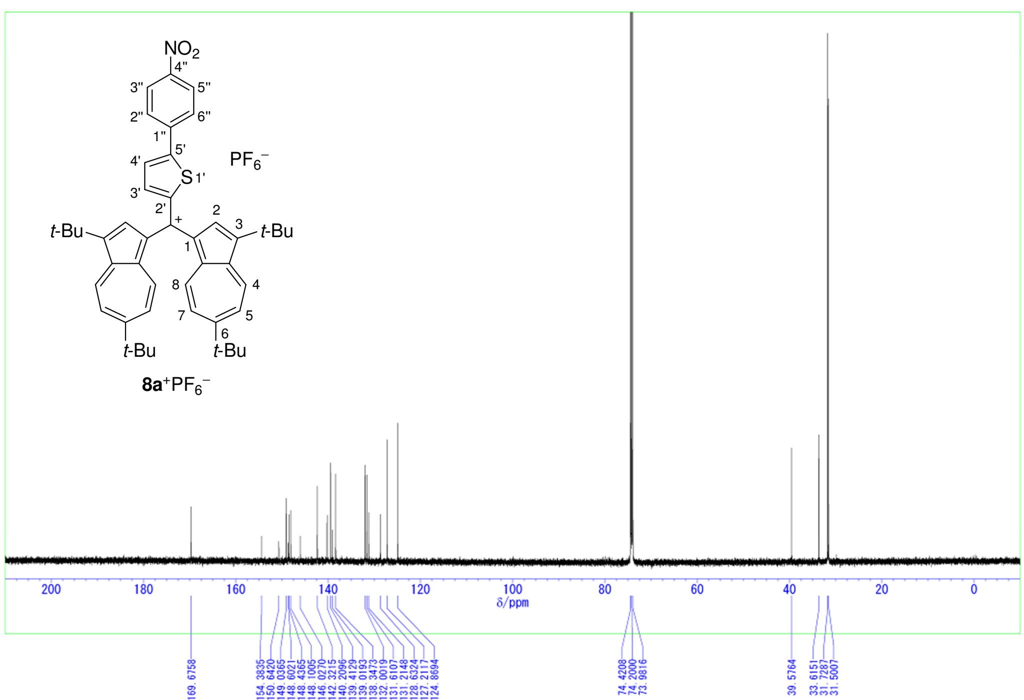

Figure S52. ^{13}C NMR spectrum (150 MHz) of bis(3,6-di-*tert*-butyl-1-azulenyl)[5-(4-nitrophenyl)-2-thienyl]methylium hexafluorophosphate ($\mathbf{8a}^{+}PF_6^{-}$) in $(CDCl_2)_2$ at 100 °C.

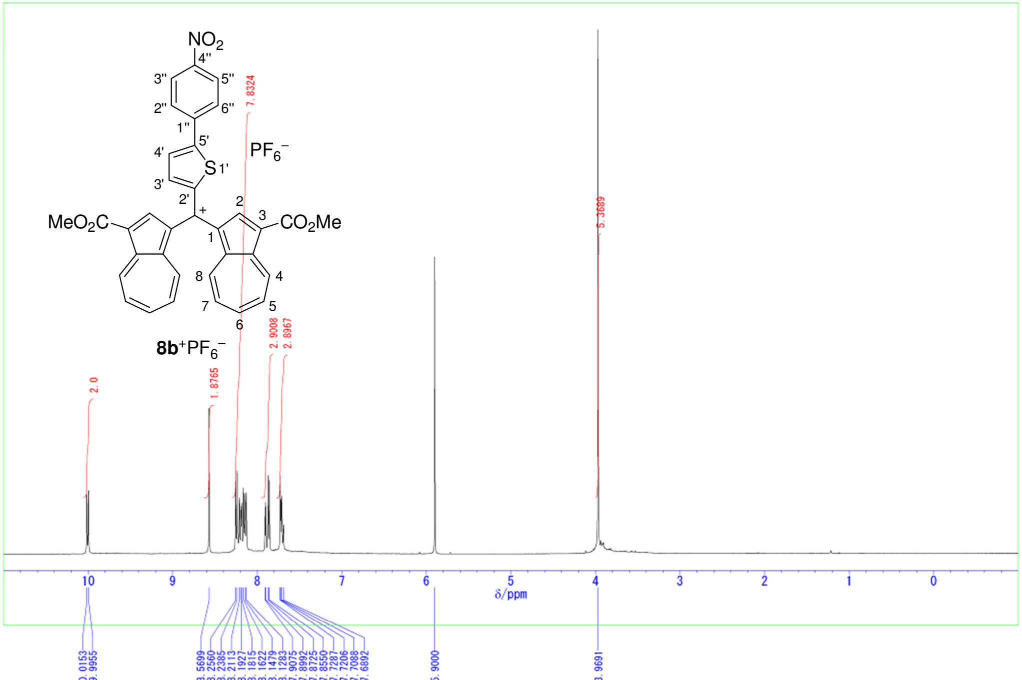

Figure S53. ^{1}H NMR spectrum (500 MHz) of bis(3-methoxycarbonyl-1-azulenyl)[5-(4-nitrophenyl)-2-thienyl]methylium hexafluorophosphate (**8b**$^{+}PF_6^{-}$) in $(CDCl_2)_2$ at 80 °C.

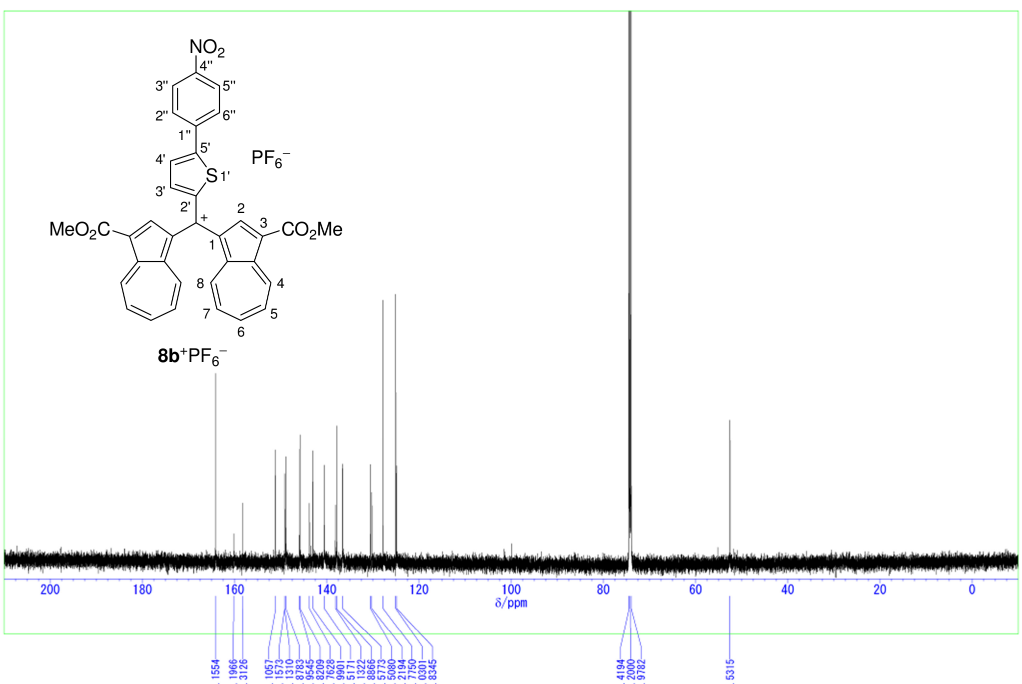

Figure S54. ^{13}C NMR spectrum (125 MHz) of bis(3-methoxycarbonyl-1-azulenyl)[5-(4-nitrophenyl)-2-thienyl]methylium hexafluorophosphate (**8b**$^{+}PF_6^{-}$) in $(CDCl_2)_2$ at 80 °C.

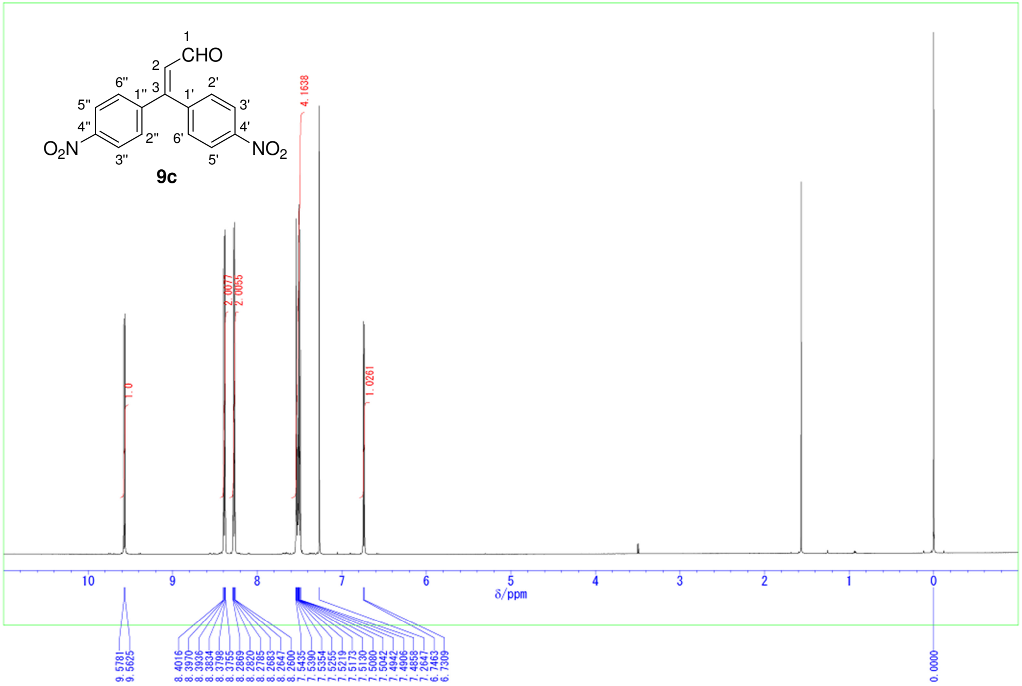

Figure S55. [1]H NMR spectrum (500 MHz) of 3,3-bis(4-nitrophenyl)-2-propenal (**9c**) in $CDCl_3$.

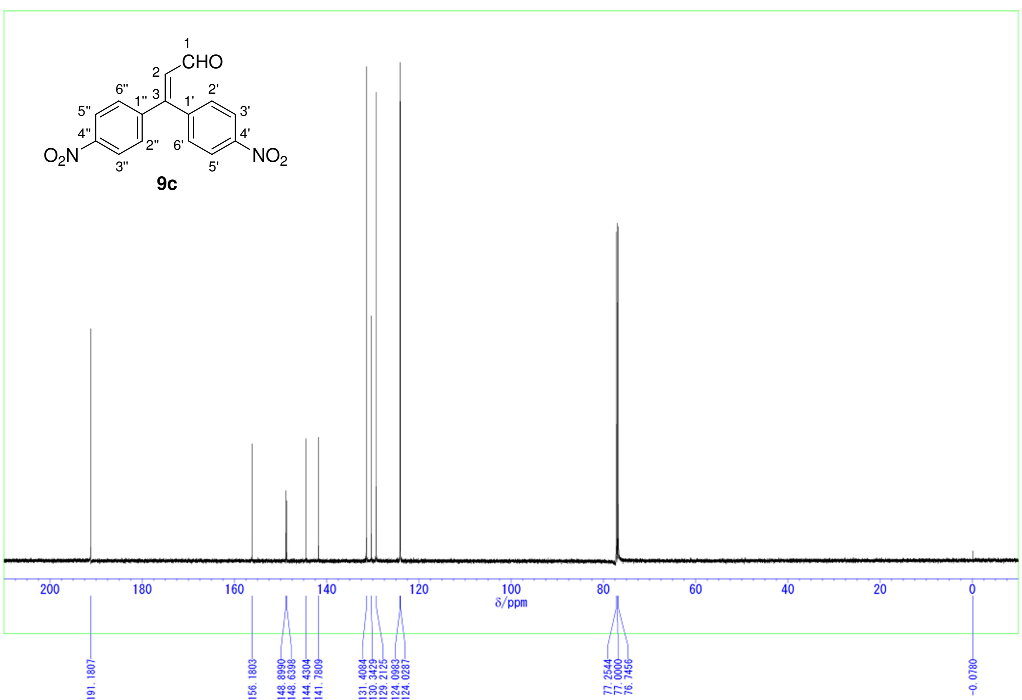

Figure S56. [13]C NMR spectrum (125 MHz) of 3,3-bis(4-nitrophenyl)-2-propenal (**9c**) in $CDCl_3$.

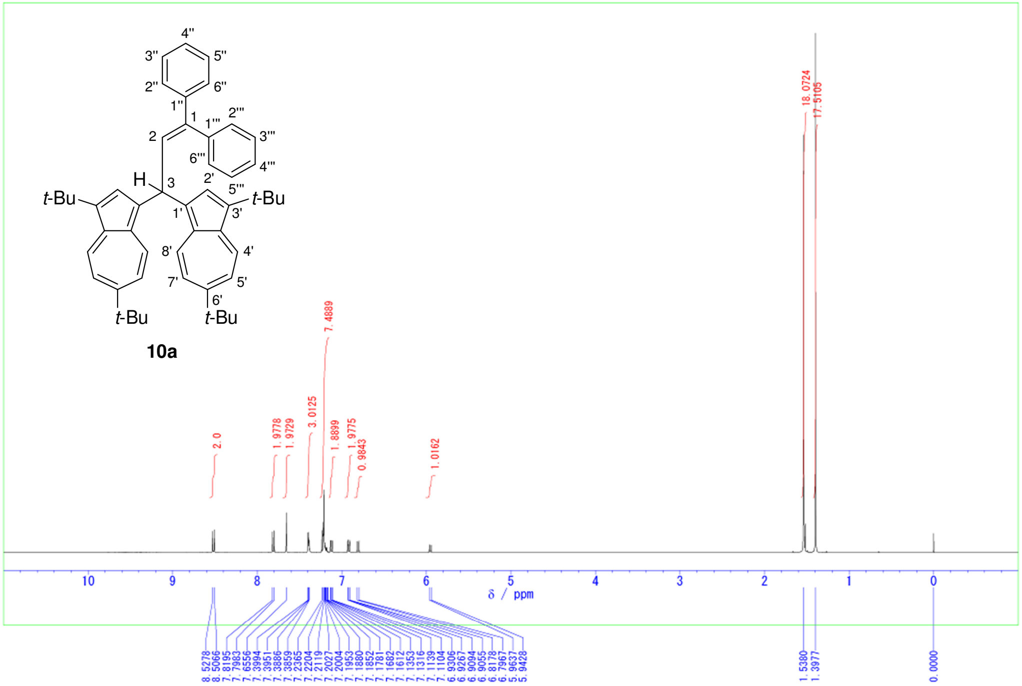

Figure S57. ^{1}H NMR spectrum (500 MHz) of 3,3-bis(3,6-di-*tert*-butyl-1-azulenyl)-1,1-diphenylpropene (**10a**) in $CDCl_3$.

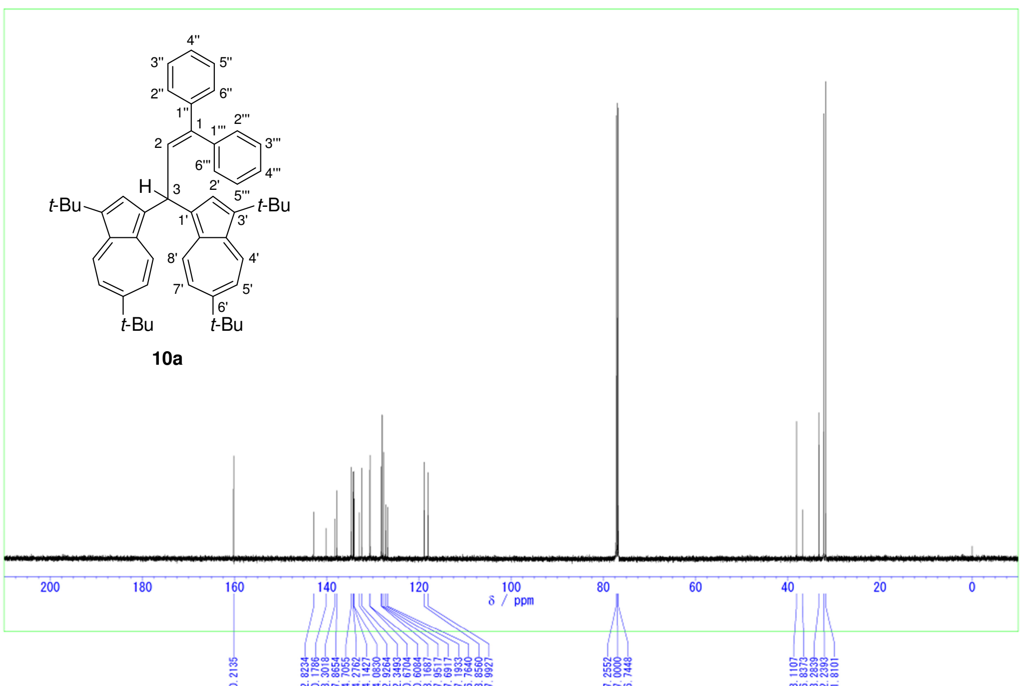

Figure S58. ^{13}C NMR spectrum (125 MHz) of 3,3-bis(3,6-di-*tert*-butyl-1-azulenyl)-1,1-diphenylpropene (**10a**) in $CDCl_3$.

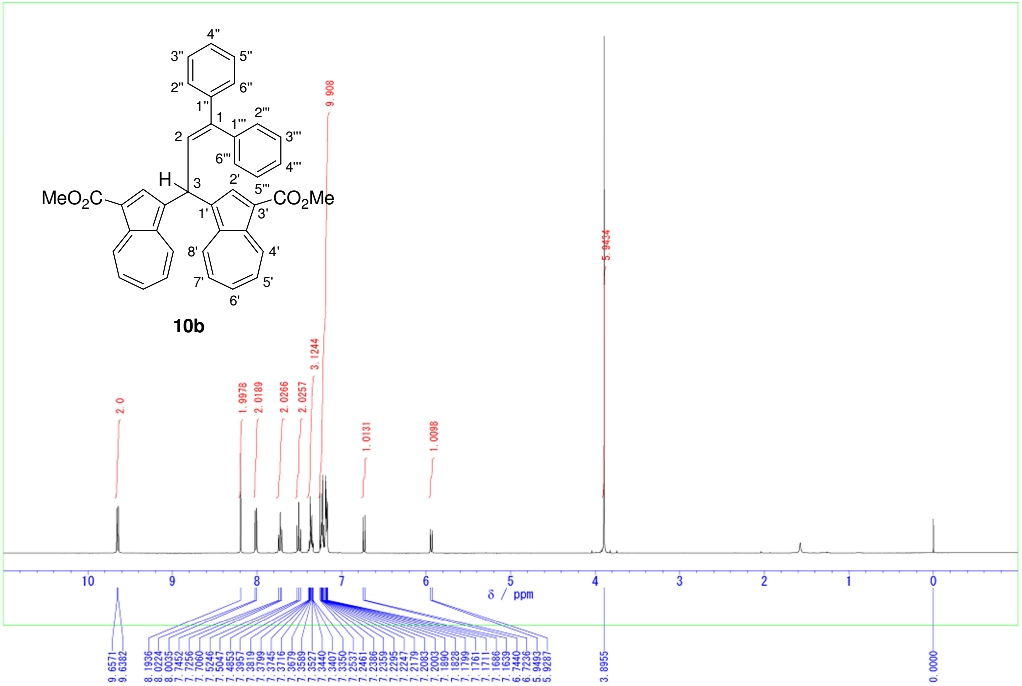

Figure S59. ^{1}H NMR spectrum (500 MHz) of 3,3-bis(3-methoxycarbonyl-1-azulenyl)-1,1-diphenylpropene (**10b**) in $CDCl_3$.

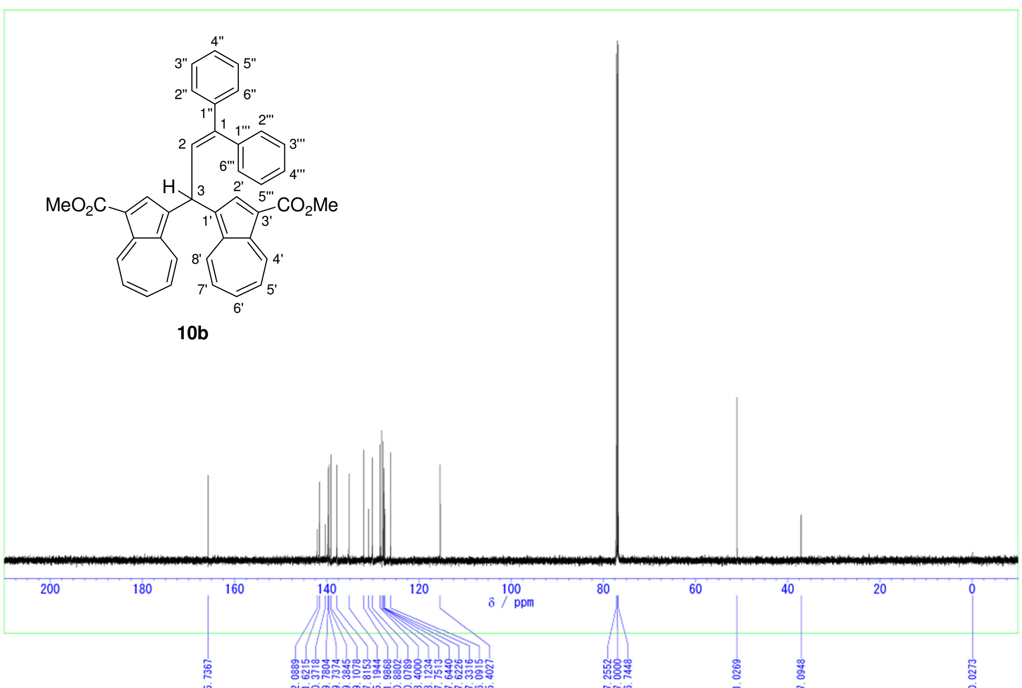

Figure S60. ^{13}C NMR spectrum (125 MHz) of 3,3-bis(3-methoxycarbonyl-1-azulenyl)-1,1-diphenylpropene (**10b**) in $CDCl_3$.

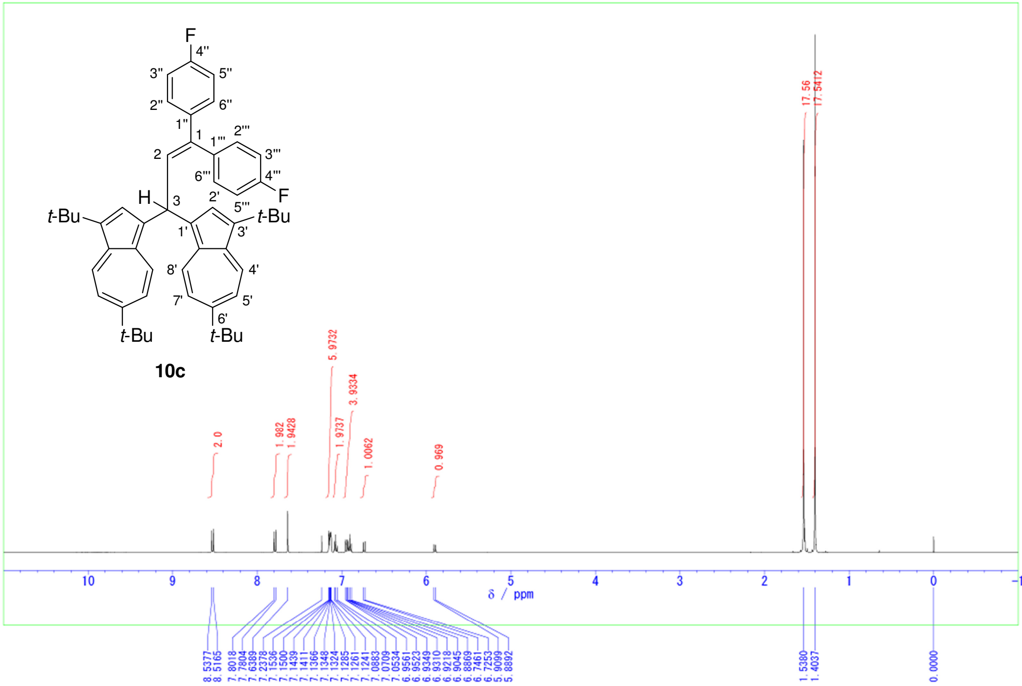

Figure S61. ^{1}H NMR spectrum (500 MHz) of 3,3-bis(3,6-di-*tert*-butyl-1-azulenyl)-1,1-bis(4-fluorophenyl)propene (**10c**) in $CDCl_3$.

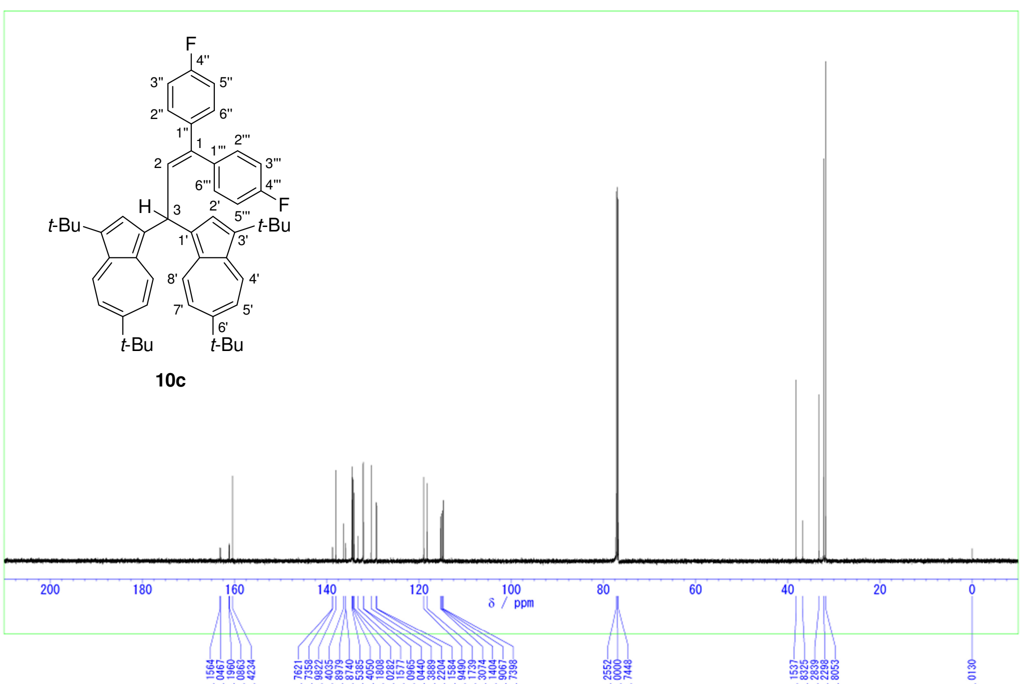

Figure S62. ^{13}C NMR spectrum (125 MHz) of 3,3-bis(3,6-di-*tert*-butyl-1-azulenyl)-1,1-bis(4-fluorophenyl)propene (**10c**) in $CDCl_3$.

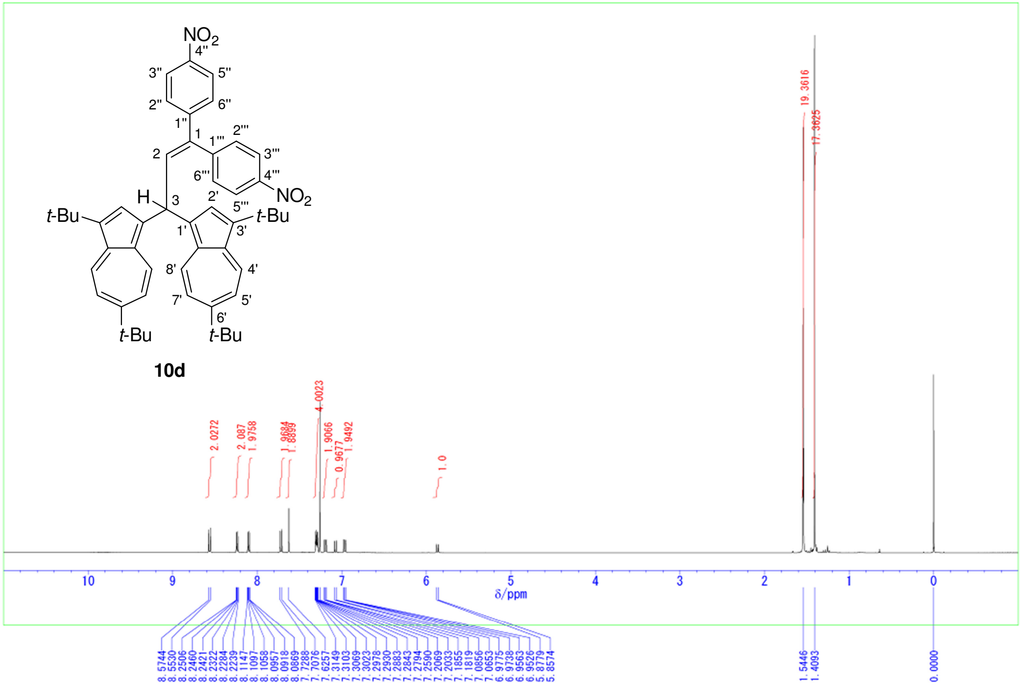

Figure S63. [1]H NMR spectrum (500 MHz) of 3,3-bis(3,6-di-*tert*-butyl-1-azulenyl)-1,1-bis(4-nitrophenyl)propene (**10d**) in $CDCl_3$.

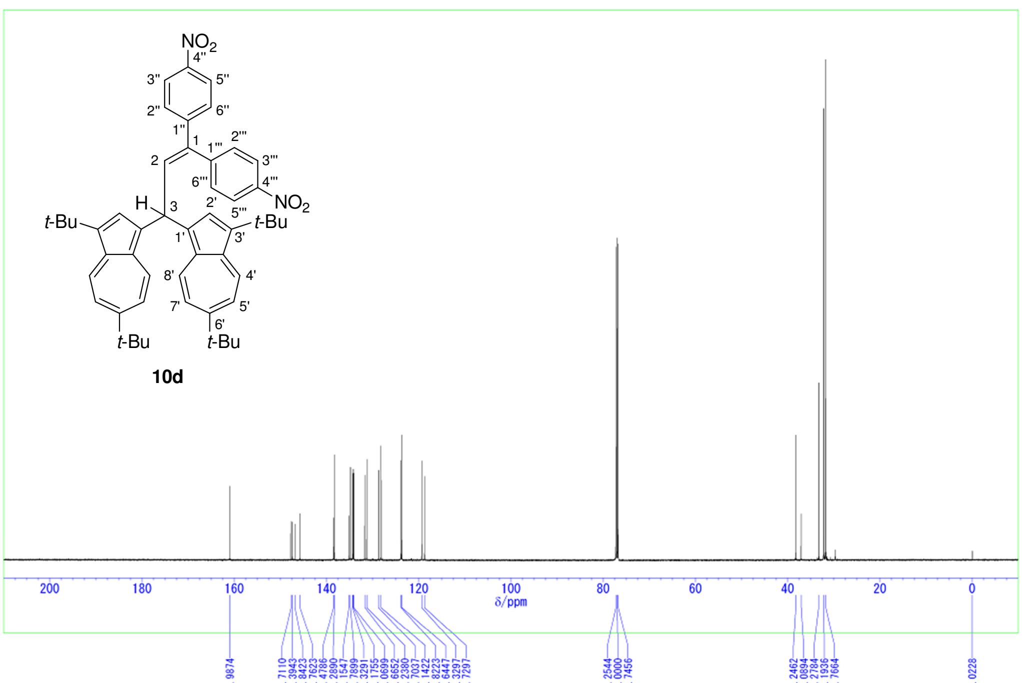

Figure S64. [13]C NMR spectrum (125 MHz) of 3,3-bis(3,6-di-*tert*-butyl-1-azulenyl)-1,1-bis(4-nitrophenyl)propene (**10d**) in $CDCl_3$.

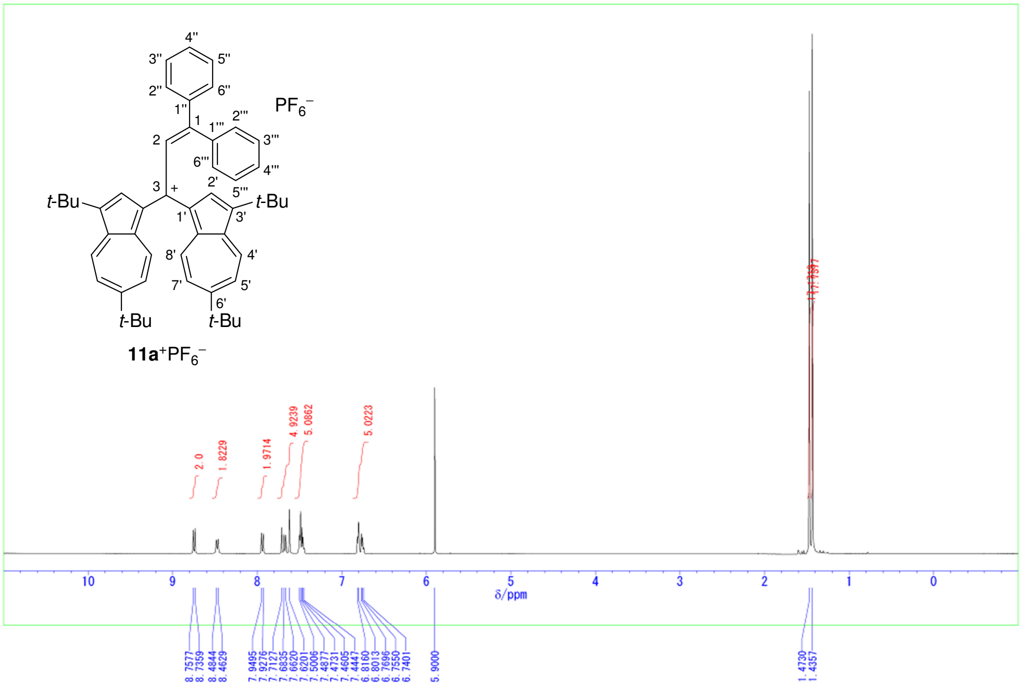

Figure S65. ^{1}H NMR spectrum (600 MHz) of 3,3-bis(3,6-di-*tert*-butyl-1-azulenyl)-1,1-diphenylpropenylium hexafluorophosphate (**11a**$^{+}$PF$_6^{-}$) in $(CDCl_2)_2$ at 120 °C.

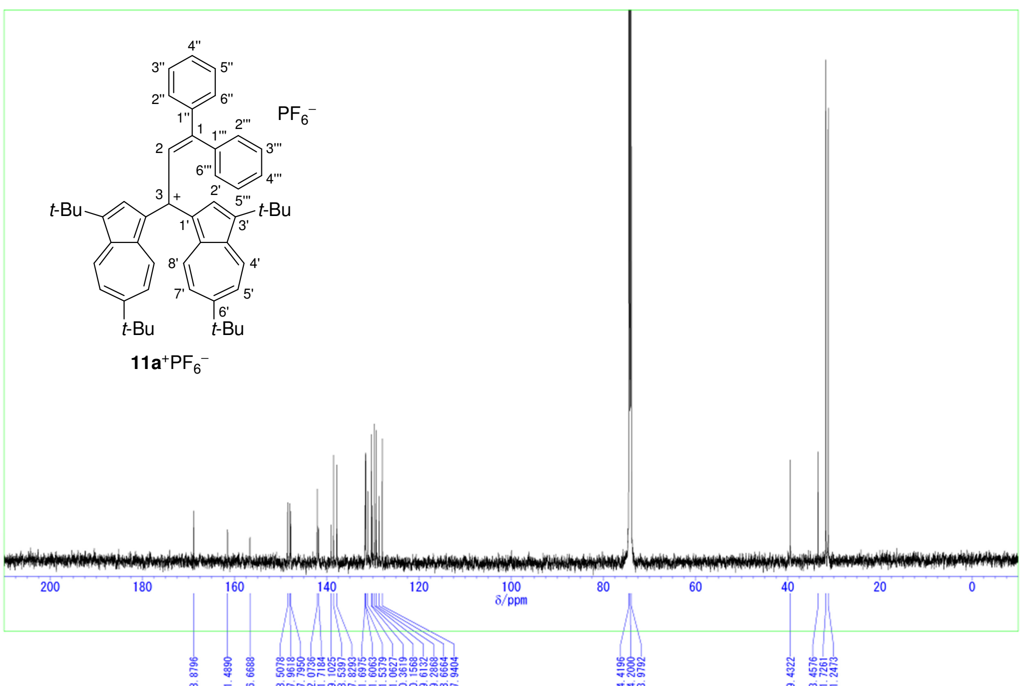

Figure S66. ^{13}C NMR spectrum (150 MHz) of 3,3-bis(3,6-di-*tert*-butyl-1-azulenyl)-1,1-diphenylpropenylium hexafluorophosphate (**11a**$^{+}$PF$_6^{-}$) in $(CDCl_2)_2$ at 120 °C.

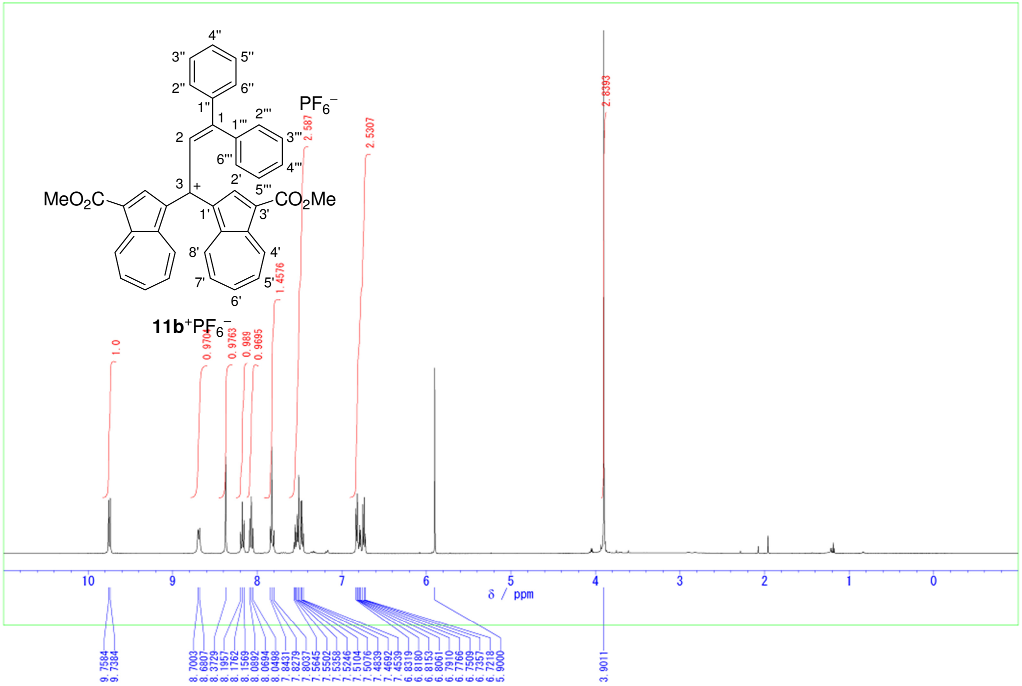

Figure S67. ^{1}H NMR spectrum (500 MHz) of 3,3-bis(3-methoxycarbonyl-1-azulenyl)-1,1-diphenylpropenylium hexafluorophosphate (**11b**$^{+}PF_6^{-}$) in $(CDCl_2)_2$ at 80 °C.

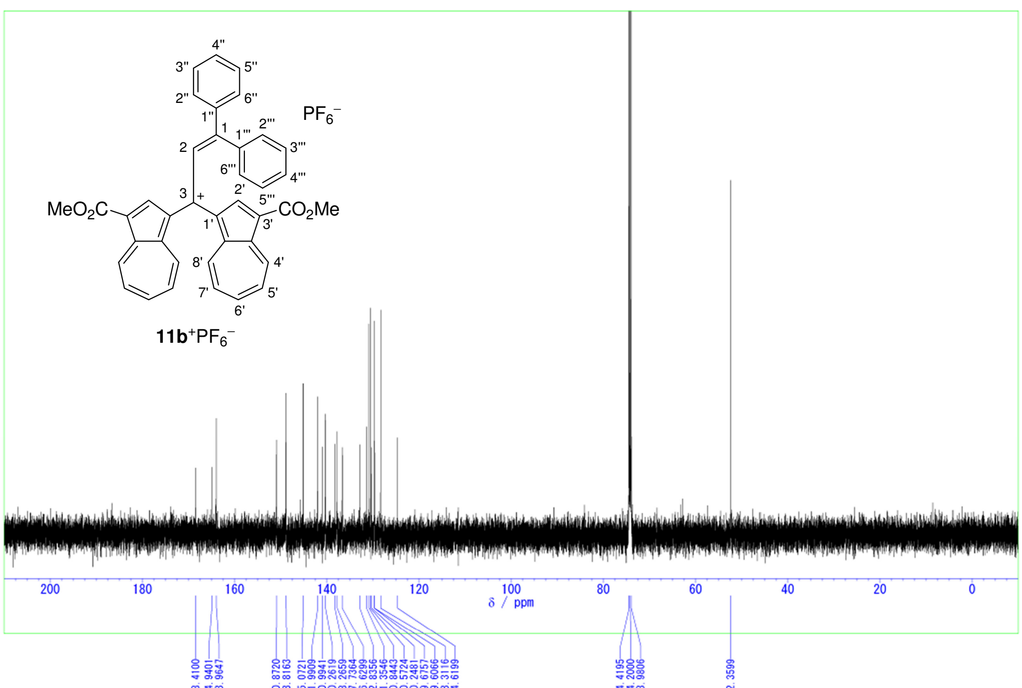

Figure S68. ^{13}C NMR spectrum (125 MHz) of 3,3-bis(3-methoxycarbonyl-1-azulenyl)-1,1-diphenylpropenylium hexafluorophosphate (**11b**$^{+}PF_6^{-}$) in $(CDCl_2)_2$ at 80 °C.

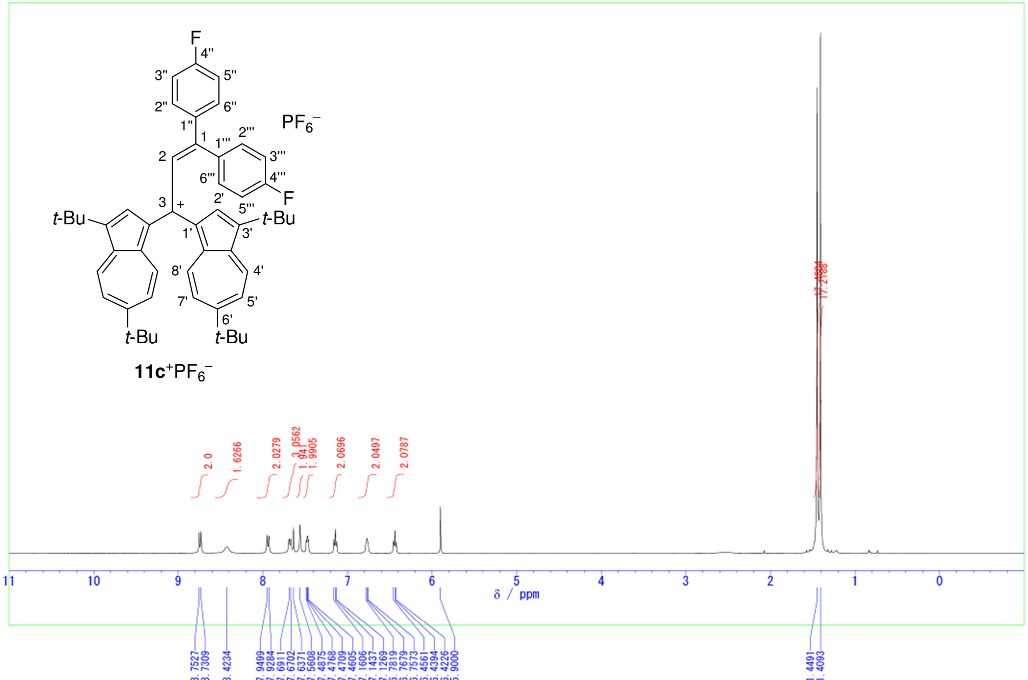

Figure S69. ^{1}H NMR spectrum (500 MHz) of 3,3-bis(3,6-di-*tert*-butyl-1-azulenyl)-1,1-bis(4-fluorophenyl)propenylium hexafluorophosphate (**11c**$^{+}PF_6^{-}$) in $(CDCl_2)_2$ at 80 °C.

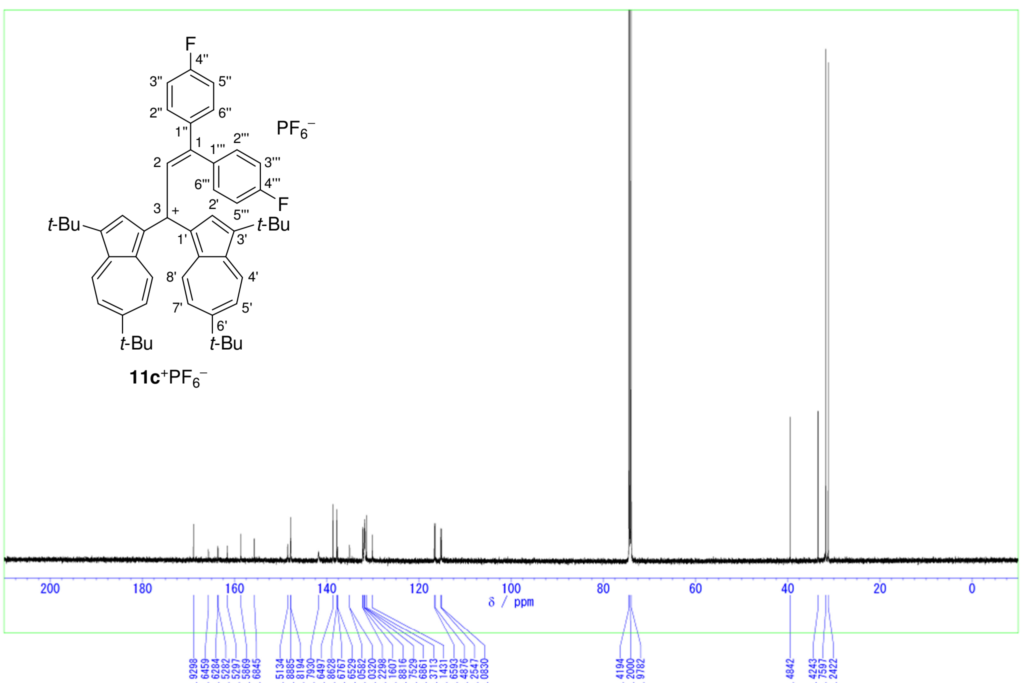

Figure S70. ^{13}C NMR spectrum (125 MHz) of 3,3-bis(3,6-di-*tert*-butyl-1-azulenyl)-1,1-bis(4-fluorophenyl)propenylium hexafluorophosphate (**11c**$^{+}PF_6^{-}$) in $(CDCl_2)_2$ at 80 °C.

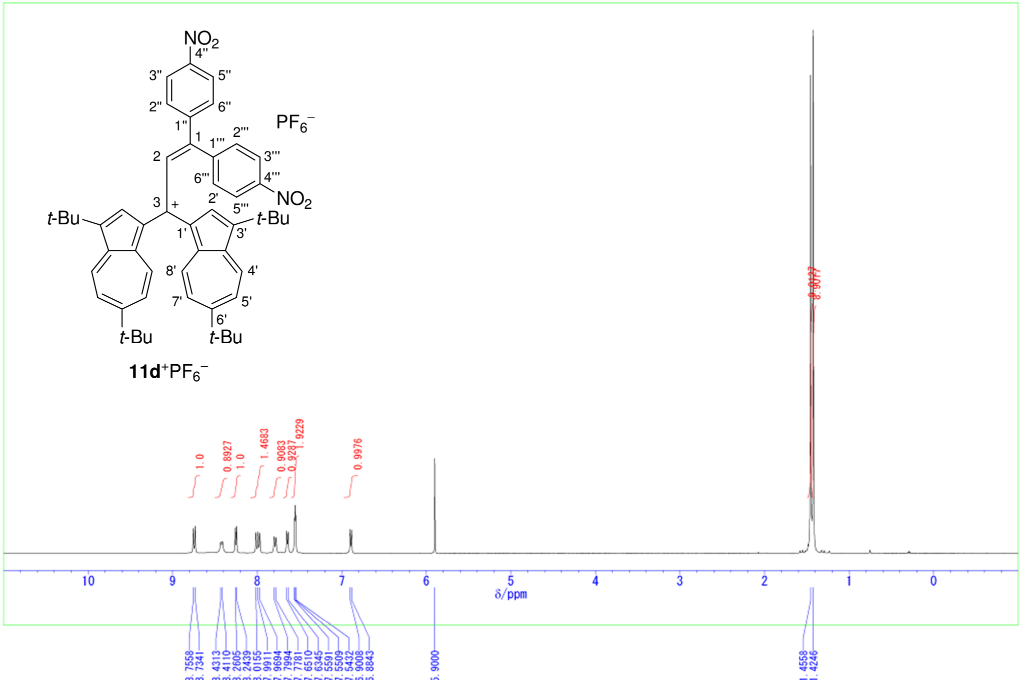

Figure S71. ^{1}H NMR spectrum (500 MHz) of 3,3-bis(3,6-di-*tert*-butyl-1-azulenyl)-1,1-bis(4-nitrophenyl)propenylium hexafluorophosphate (**11d**$^{+}PF_6^{-}$) in $CDCl_3$.

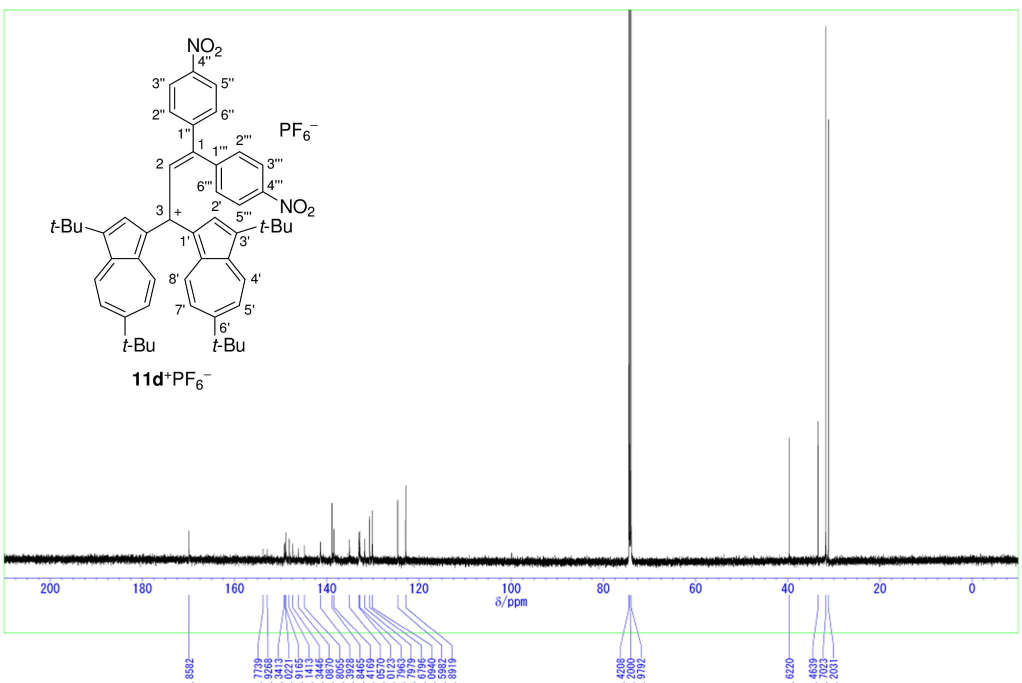

Figure S72. ^{13}C NMR spectrum (125 MHz) of 3,3-bis(3,6-di-*tert*-butyl-1-azulenyl)-1,1-bis(4-nitrophenyl)propenylium hexafluorophosphate (**11d**$^{+}PF_6^{-}$) in $CDCl_3$.

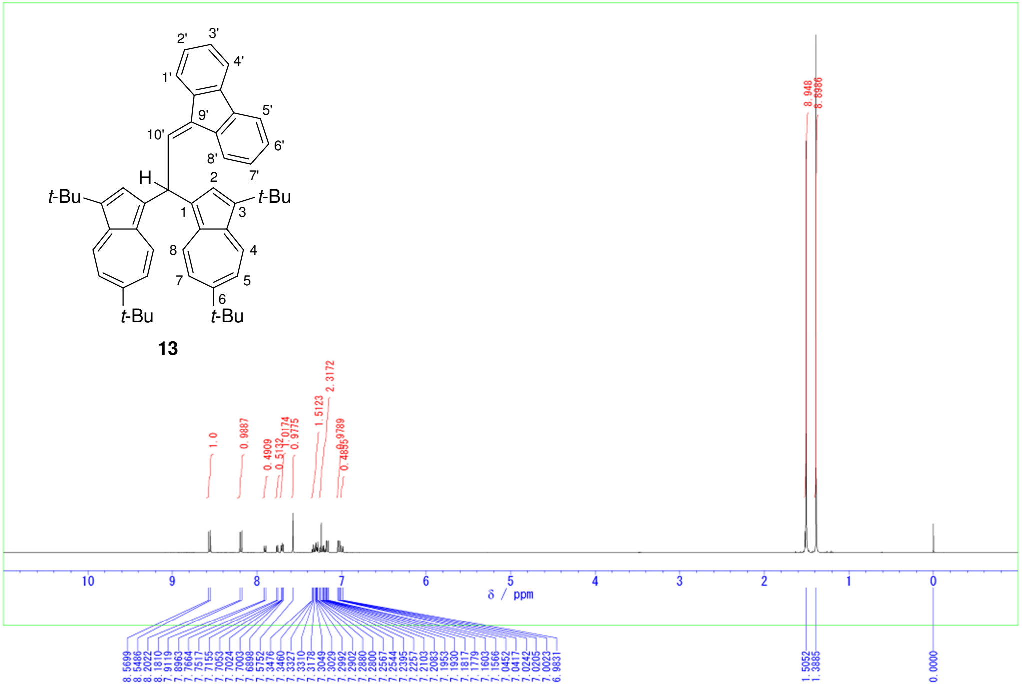

Figure S73. ^{1}H NMR spectrum (500 MHz) of 9-[2,2-bis(3,6-di-*tert*-butyl-1-azulenyl)ethylidene]-9*H*-fluorene (**13**) in $CDCl_3$.

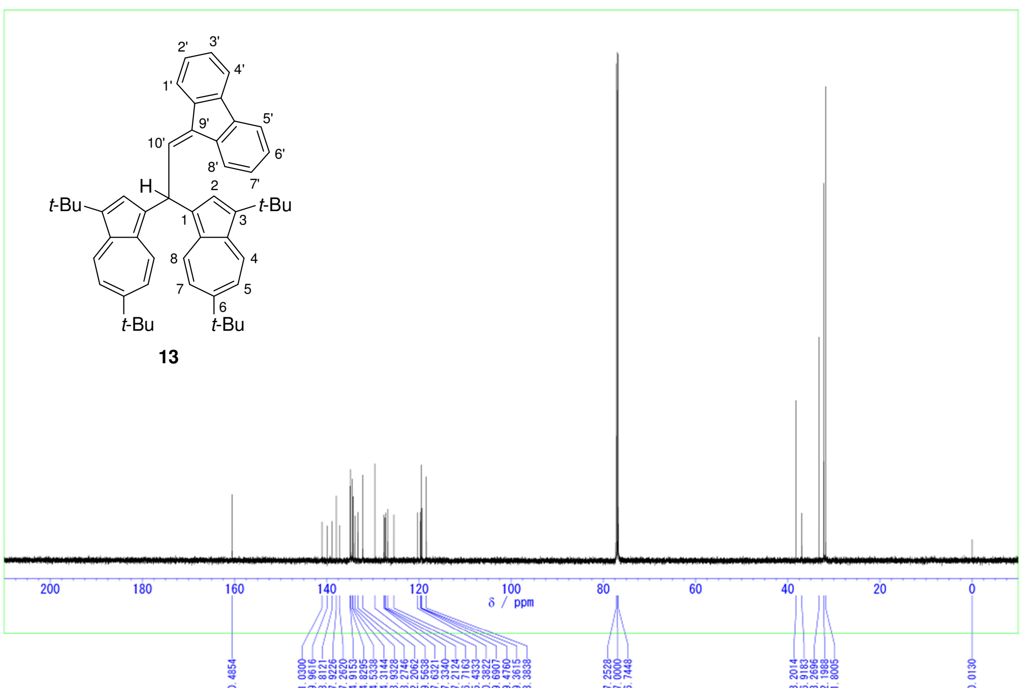

Figure S74. ^{13}C NMR spectrum (125 MHz) of 9-[2,2-bis(3,6-di-*tert*-butyl-1-azulenyl)ethylidene]-9*H*-fluorene (**13**) in $CDCl_3$.

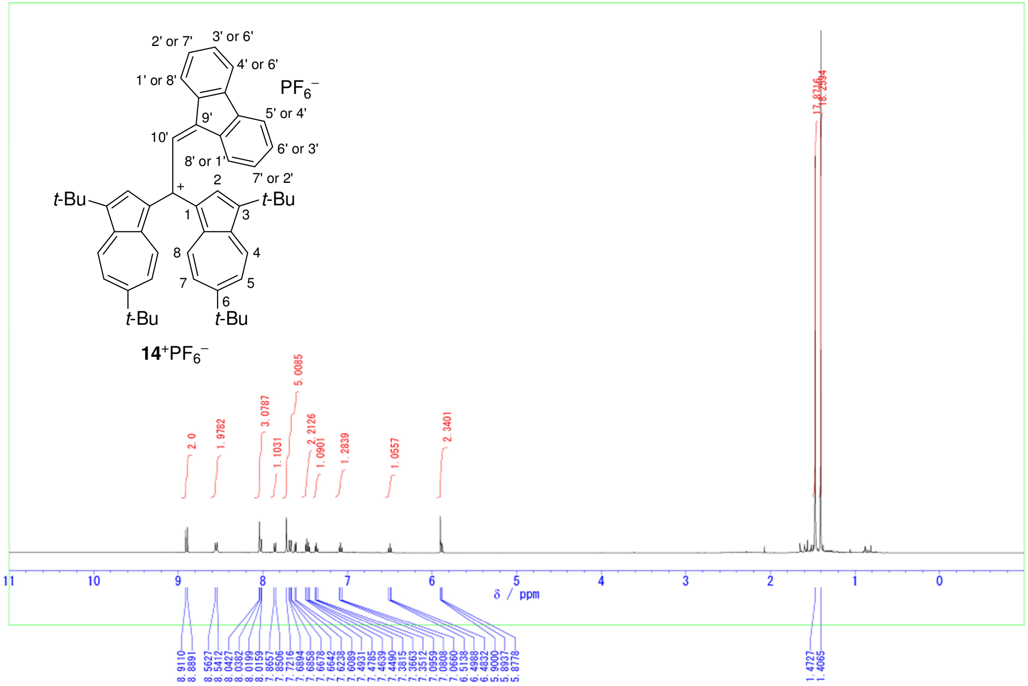

Figure S75. ^{1}H NMR spectrum (500 MHz) of 1,1-bis(3,6-di-*tert*-butyl-1-azulenyl)-2-(9*H*-fluorenylidene)ethylium hexafluorophosphate ($\mathbf{14}^{+}PF_6^{-}$) in $(CDCl_2)_2$ at 80 °C.

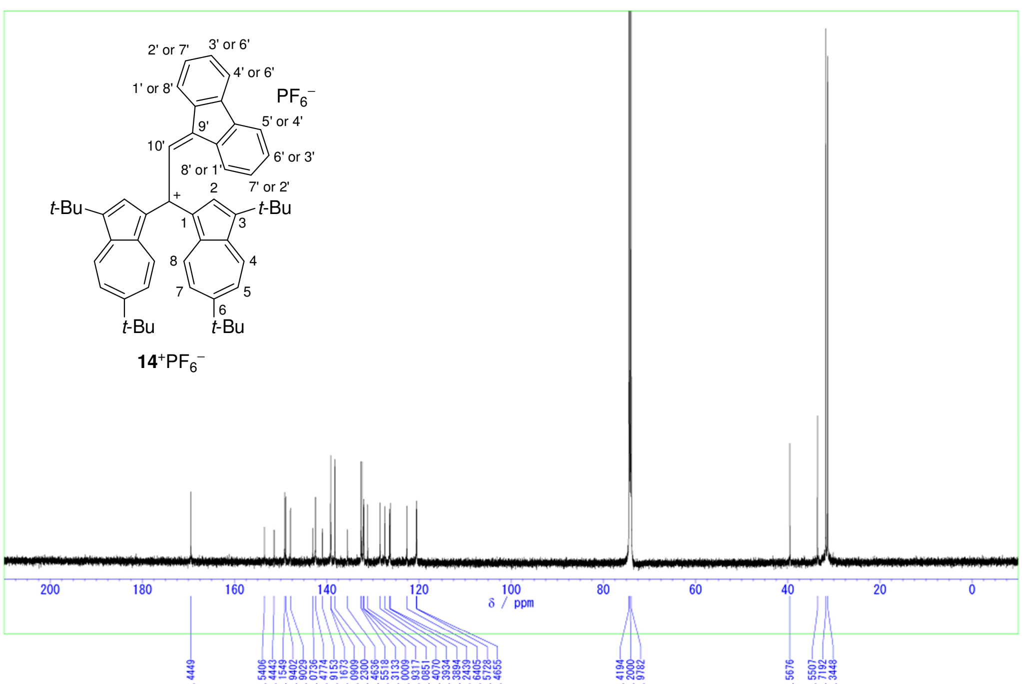

Figure S76. ^{13}C NMR spectrum (125 MHz) of 1,1-bis(3,6-di-*tert*-butyl-1-azulenyl)-2-(9*H*-fluorenylidene)ethylium hexafluorophosphate ($\mathbf{14}^{+}PF_6^{-}$) in $(CDCl_2)_2$ at 80 °C.

